Molecular Biology of the Cell
Vol. 20, 4091–4106, September 15, 2009

Regulation of Cell Death by Recycling Endosomes and Golgi Membrane Dynamics via a Pathway Involving Src-family kinases, Cdc42 and Rab11a

Marie-Claude Landry, Andréane Sicotte, Claudia Champagne, and Josée N. Lavoie

Centre de Recherche en Cancérologie de l'Université Laval, L'Hôtel-Dieu de Québec, Centre de Recherche du Centre Hospitalier Universitaire de Quebec, Québec G1R 2J6, Canada

Submitted January 21, 2009; Revised July 9, 2009; Accepted July 17, 2009
Monitoring Editor: Donald D. Newmeyer

Actin dynamics and membrane trafficking influence cell commitment to programmed cell death through largely undefined mechanisms. To investigate how actin and recycling endosome (RE) trafficking can engage death signaling, we studied the death program induced by the adenovirus early region 4 open reading frame 4 (E4orf4) protein as a model. We found that in the early stages of E4orf4 expression, Src-family kinases (SFKs), Cdc42, and actin perturbed the organization of the endocytic recycling compartment and promoted the transport of REs to the Golgi apparatus, while inhibiting recycling of protein cargos to the plasma membrane. The resulting changes in Golgi membrane dynamics that relied on actin-regulated Rab11a membrane trafficking triggered scattering of Golgi membranes and contributed to the progression of cell death. A similar mobilization of RE traffic mediated by SFKs, Cdc42 and Rab11a also contributed to Golgi fragmentation and to cell death progression in response to staurosporine, in a caspase-independent manner. Collectively, these novel findings suggest that diversion of RE trafficking to the Golgi complex through a pathway involving SFKs, Cdc42, and Rab11a plays a general role in death signaling by mediating regulated changes in Golgi dynamics.

INTRODUCTION

Cell death (CD) mechanisms rely on the orderly remodeling of the cell cytoskeleton and membranes through the trafficking of proteins and lipids to distinct cellular organelles (Garofalo *et al*., 2007; Tembe and Henderson, 2007). This movement of proteins and lipids from one compartment to another serves to relay death signals in part through modifications of organelle dynamics. Growing evidence indicates that different organelles can sense specific stress and initiate CD signaling once a critical threshold of damage has been reached (Ferri and Kroemer, 2001). For example, the Golgi complex has been shown to undergo major changes in structural organization associated with the release of peripheral proteins that seems to acquire death-inducing functions (Hicks and Machamer, 2005). Hence, different organelles are simultaneously engaged in dynamic changes induced by death signaling, and interorganellar cross-talks have emerged as a fundamental issue in the field of CD. Little is known, however, regarding how such dynamic changes are orchestrated. Considering the key function of actin in membrane trafficking and in the maintenance of organelle integrity (Egea *et al*., 2006; Lanzetti, 2007), it is conceivable that local changes in the dynamic state of actin play a role. Such a function for actin has remained enigmatic, owing to the lack of a CD model involving organelle-based actin dynamics.

We have shown that the 14-kDa protein encoded by the early region 4 open reading frame 4 (E4orf4) of human adenoviruses triggers CD in part through regulated changes in actin dynamics (Robert *et al*., 2006). When expressed in a wide variety of transformed and cancer cell lines, E4orf4 activates a CD pathway associated with apoptotic hallmarks, including dynamic blebbing, chromatin condensation and pyknosis; however, CD resists to a variety of caspase inhibitors and does not depend on the function of p53 and Bcl-2-family of proteins (Lavoie *et al*., 1998; Marcellus *et al*., 1998; Shtrichman *et al*., 1999; Lavoie *et al*., 2000; Livne *et al*., 2001; Robert *et al*., 2002, 2006; Smadja-Lamere *et al*., 2008). It was shown that E4orf4 accumulation on cortical and perinuclear membranes marks the onset of a polarized remodeling of the actin cytoskeleton, which is associated with massive recruitment of recycling endosomes (REs) and a lethal increase in cell tension (Robert *et al*., 2006; Smadja-Lamere *et al*., 2008). These dynamic cytoskeletal changes are controlled by several pathways involving Rho GTPases, including the Cdc42/N-Wasp/Arp2/3 signaling axis that stimulates the formation of dynamic actin particles associated with REs (Robert *et al*., 2006). Src-family kinases (SFKs) also play a key role in activating the death program, through their binding to E4orf4 and phosphorylation of discrete Tyr

This article was published online ahead of print in *MBC in Press* (http://www.molbiolcell.org/cgi/doi/10.1091/mbc.E09–01–0057) on July 29, 2009.

Address correspondence to: Josée N. Lavoie (josee.lavoie@crhdq.ulaval.ca).

Abbreviations used: EE, early endosome; ERC, endocytic recycling compartment; E4orf4, early region 4 open reading frame 4; GalT, β-1,4-galactosyl transferase; LatA, latrunculin A; mRFP, monomeric red fluorescent protein; CD, cell death; PNS, postnuclear supernatant; RE, recycling endosome; SDCM, spinning disk confocal microscopy; SFK, Src-family kinase; STS, staurosporine; STxB, Shiga toxin subunit-B; Tf, transferrin; TfR, transferrin receptor; TGN, *trans*-Golgi network; VSVG-ts, temperature-sensitive mutant of the vesicular stomatitis virus G protein; wCRIB, CRIB domain of N-Wasp.

motifs (Lavoie *et al*., 2000; Gingras *et al*., 2002; Champagne *et al*., 2004). In turn, phosphorylated E4orf4 diverts SFK-dependent signaling, favoring the tyrosine phosphorylation of a subset of targets that presumably contribute to deregulate endosomal actin dynamics (Robert *et al*., 2006). However, the relationship between SFKs and Cdc42 and their impact on RE trafficking remain unclear, like the functional relevance of RE trafficking to the death process. Hence, E4orf4 offers a unique model for studying the role of actin-regulated membrane trafficking in CD signaling. Given that E4orf4 is one of a family of proteins exhibiting a so-called tumor cell-selective killing activity, the mechanism involved is of great interest (Shtrichman *et al*., 1999; Bruno *et al*., 2009).

The REs are a heterogeneous population of tubulovesicular endosomes typically condensed in the pericentriolar region, which forms the endocytic recycling compartment (ERC) (Saraste and Goud, 2007). The traffic of REs is controlled by the small GTPase Rab11 and is mainly involved in the slow retrieval of internalized membranes and signaling molecules to the plasma membrane or to the *trans*-Golgi (TGN) via retrograde membrane transport (van Ijzendoorn, 2006). The ERC seems to represent a center integrating vesicular transport with signaling modules controlling actin remodeling and could provide an intracellular reservoir of membranes that would be readily recruited during dynamic rearrangement of the cell (Jones *et al*., 2006; Saraste and Goud, 2007). For example, the actin polymerization complex Cdc42/N-Wasp is assembled at the ERC (Parsons *et al*., 2005) and Src activation (which has potent effects on actin) is tightly linked to its transport from the ERC to peripheral membrane sites through a pathway involving Rab11, actin, and Rho GTPases (Sandilands *et al*., 2004; Sandilands and Frame, 2008). It is currently unknown, however, whether SFKs and Rho GTPases can contribute to mobilize REs during cell activation processes. Indeed, studies of the function of Rab11 suggest that cells mobilize REs for delivering membranes, actin and signaling molecules to membrane regions subjected to a dynamic reorganization (van Ijzendoorn, 2006). It has been shown recently that death receptor signaling leads to an accumulation of REs in the peri-Golgi region in T cells (Degli Esposti *et al*., 2009), suggesting that REs could be mobilized during CD. Whether REs could contribute to the remodeling of actin and organelles taking place during the execution of CD pathways has not been explored (Ndozangue-Touriguine *et al*., 2008).

In the present study, we have investigated whether regulated changes in actin associated with RE trafficking could modulate CD by influencing organelle dynamics, by using E4orf4 as a prototype model and staurosporine as a classical apoptotic trigger. Moreover, we have explored the connecting route between REs and the Golgi complex as a mechanism coupling RE trafficking to CD signaling via structural changes of the Golgi. We present evidence for a model in which a pathway involving SFKs, Cdc42, actin, and Rab11a controls the mobilization of REs during CD, promoting the transport of REs to Golgi membranes that in turn trigger caspase-independent changes in Golgi dynamics involved in the progression of cell death.

MATERIALS AND METHODS

Expression Vectors, Antibodies, and Chemicals

Expression vectors used in this study are described in Supplemental Data. Those described previously and the chemicals used are listed in Supplemental Table S1. The commercial antibodies used are listed in Supplemental Table S2. The rabbit anti-TOM20 was a gift from G. Shore (McGill University, Montreal, QC, Canada), and the rabbit anti-extracellular signal-regulated kinase (ERK) 2 was described previously (Huot *et al*., 1995).

Cell Culture, Transfection, and Small Interfering RNA (siRNA)

HeLa (Jones *et al*., 1971) and MCF7 (Soule *et al*., 1973) cell lines were maintained in α-minimal essential medium (MEM) and 10% fetal bovine serum, and 293T cells (Graham *et al*., 1977) were grown in DMEM and 10% fetal bovine serum. MCF7 and HeLa cells were transfected with Lipofectamine 2000 (Invitrogen, Carlsbad, CA), according to the manufacturer's recommendations. 293T cells were transfected by the calcium-phosphate method (Lavoie *et al*., 2000). For siRNA experiments, HeLa and MCF7 cells were transfected overnight by the calcium-phosphate method or using the TransIT-TKO reagent (Mirus Bio, Madison, WI), split for subsequent transfection 48 h later, and examined 72 h later. The commercial siRNA oligonucleotides used in this study are listed in Supplemental Table S2. For experiments in E4orf4-expressing cells, chemical inhibitors SKI-1 (10 μM), PP2 (10 μM), SU6656 (5 μM), NSC23766 (100 μM), Q-VD-OPh (10 μM), and zVAD-FMK (50 μM) or the vehicles were added to the culture medium 4–5 h after transfection, but before the onset of E4orf4 expression. For experiments using staurosporine (STS), caspase inhibitors and other drugs were added to culture medium 1 h before and remained during STS treatment (1 μM). Latrunculin A (LatA) was used at 1 μM or at a lower concentration (0.5 μM) that inhibits actin dynamics without disrupting the actin cytoskeleton. Brefeldin-A was used at 5 μg/ml to induce the massive Golgi-to-endoplasmic reticulum (ER) retrograde transport of membranes.

Cell Fractionation and Western Blot

For isolation of heavy/light membranes, cells were suspended at 50×10^6 cells/ml in sucrose buffer (20 mM HEPES, pH 7.5, 250 mM sucrose, 10 mM KCl, 1.5 mM $MgCl_2$, 1 mM EDTA, 1 mM EGTA, 15 μg/ml leupeptin, 5 μg/ml aprotinin, 1 μg/ml pepstatin A, 1 mM phenylmethylsulfonyl fluoride, and 1 mM Na_3VO_4), swollen on ice for 1 h, and forced through a 27-gauge needle 50–60 times (Robert *et al*., 2006). Post nuclear supernatants (PNSs) were pelleted at $700 \times g$ and further fractionated by serial centrifugation (heavy membranes, $8000 \times g$; light membranes, $170{,}000 \times g$). For analysis of Rab11a distribution, the homogenized cells were centrifuged at $5000 \times g$, and supernatants were centrifuged at $170{,}000 \times g$ for 30 min to obtain the membrane and cytosolic fractions. To obtain a 10–20-30% linear gradient of Opti-Prep (iodixanol), the homogenized cells were centrifuged at $700 \times g$, and PNSs (1 ml) were mixed with Opti-Prep (1.5 ml of 50% solution) to reach a final concentration of 30% iodixanol. The mixtures were layered under 1.3 ml of 20% iodixanol and 1.2 ml of 10% iodixanol, respectively, as described previously (Chen *et al*., 2006). The gradient was spun at $360{,}000 \times g$ for 3 h at 4°C and collected into 20 fractions. Equal volumes of fractions were loaded on SDS-polyacrylamide gel electrophoresis gels, and Western blots were performed as described previously (Lavoie *et al*., 2000). Protein concentrations were determined with the DC Protein Assay (Bio-Rad Laboratories, Hercules, CA), and densitometric analyses were performed from FluorS MAX Multi-imager–captured images using Quantity 1-D software, version 4.6.0 (Bio-Rad Laboratories).

Immunofluorescence and Membrane Trafficking Assays

DNA was stained with cell-permeable Hoechst before cell fixation. Caspase activities were visualized in a single cell by using a cell-permeant generic rhodamine-based caspase substrate (D2-R110; Invitrogen), which is converted to a fluorescent R110 cleavage product by caspases. The D2-R110 caspase substrate was added to a concentration of 50 μM 2 h before visualization in live cells by epifluorescence. Cells fixation was performed in 3.7% formaldehyde in Luftig buffer [0.2 M sucrose, 35 mM piperazine-*N*,*N*′-bis(2-ethanesulfonic acid), pH 7.4, 5 mM EGTA, and 5 mM $MgSO_4$] for 20 min at 37°C, and fixation-induced fluorescence was quenched with 50 mM NH_4Cl for 15 min at room temperature (RT). Immunostaining was performed as described previously (Lavoie *et al*., 2000). For Rab11a staining, cells were fixed and incubated in 30% sucrose for 2 h before permeabilization by four cycles of freeze/thaw (30 s in liquid nitrogen followed by 1 min at room temperature). Analyses of mitochondrial transmembrane potential ($\Delta\psi m$) were performed by incubating cells with 25 nM MitoTracker Deep Red for 20 min at 37°C before cell fixation. To determine an average $\Delta\psi m$/cell, the ratio between mitochondrial total fluorescence intensity over the total area of the mitochondrial network was measured from confocal image stacks by using the Measure Integrated Density function of the ImageJ software (National Institutes of Health, Bethesda, MD). The average loss of $\Delta\psi m$ (in percent) was obtained from the ratio between the average $\Delta\psi m$/cell of E4orf4-expressing cells over the average $\Delta\psi m$/cell of E4orf4-negative cells for each individual experiment (sample) to minimize the variability due to differences in staining intensity. For the labeling of ERC with Tf, cells were starved 30 min in α-MEM containing 0.5% bovine serum albumin and incubated with 5 μg/ml Alexa-647– or 488–conjugated Tf (Invitrogen) for 1 h in complete culture media. Under these conditions, Tf was predominantly localized to Rab11-positive REs. Recycling of transferrin (Tf) and MHCI from the ERC to the plasma membrane was measured as described previously (Weigert and Donaldson, 2005). HeLa cells were serum starved for 30 min at 37°C in α-MEM containing 0.5% bovine serum albumin and incubated with 5 μg/ml Alexa-488-Tf or 50 μg/ml MHCI

antibody for 30 min at 37°C. To remove protein cargos that were not internalized, cells were incubated at RT for 30 s with stripping buffer (0.5% acetic acid and 0.5 M NaCl, pH 3.0). Cells were washed twice in Luftig buffer, twice in α-MEM, and fixed (T = 0 min) or incubated in complete MEM for 30 min at 37°C (T = 30 min). Recycled cargos were removed by a second incubation with stripping buffer to reveal the internal pools only. MHCI antibody was immunodetected with an Alexa-488—conjugated goat anti-mouse in the presence of 0.2% saponin. The total fluorescence intensity of Tf or MHCI internal pools within individual cells was quantified from confocal image stacks covering the depth of the cell, using the Measure Integrated Density function of the ImageJ software. Recycling of cargos is expressed as the loss of internal fluorescence intensity (Tf or MHCI) at T = 30 min over the total fluorescence intensity at T = 0 min (in percent). The retrograde transport from early endosome (EE)/RE to the TGN was measured using recombinant B-subunit of Shiga toxin as protein cargo (StxB), as described previously (Mallard *et al.*, 1998). HeLa cells were incubated with 1 μg/ml Alexa-488-conjugated-STxB (kindly provided by Dr. L. Johannes (Institut Curie, Paris, France) for 45 min at 4°C, washed three times with ice-cold medium to remove unbound STxB, and shifted to 37°C. A short internalization period was used (20 min) to measure an increase in the rate of STxB transport to the TGN. The localization of STxB to the TGN was determined by immunostaining of endogenous golgin-97. To determine the fraction of TGN-associated STxB (in percent), the ratio between total fluorescence intensity in the TGN area over whole cell total fluorescent contents was measured from confocal image stacks using the Measure Integrated Density function of the ImageJ software. Post-Golgi transport was measured using a temperature-sensitive (ts) mutant of the vesicular stomatitis virus G protein as protein cargo (VSVG-ts-green fluorescent protein [GFP]) (Presley *et al.*, 1997). In brief, cells transfected with the VSVG-ts-GFP were incubated at 39.5°C for 16 h to allow the accumulation of VSVG protein at the ER. Cells were shifted to the permissive temperature (31.5°C) for the indicated time in the presence of cyclohexamide (75 μM) and processed for immunofluorescence of markers of the ER (calnexin) or *cis*-Golgi (GM130). The fraction of juxtanuclear/Golgi-associated VSVG-ts-GFP was estimated (in percent) by measuring the ratio between the average fluorescence intensity in the juxtanuclear area over total cell fluorescence intensity using the Measure Average Intensity function of the ImageJ software.

Microscopy, Quantitative Cellular Imaging, and Image Processing/Analyses

Epifluorescence microscopy was performed with a Nikon TE-2000 inverted microscope (60× oil 0.6–1.25 numerical aperture [NA], CoolSNAP HQ cooled charge-coupled device camera; Photometrics, Tucson, AZ) driven by MetaMorph software, version 7.14 (Molecular Devices, Sunnyvale, CA). Confocal microscopy of live and fixed cells was performed with an FV1000 confocal microscope (100× oil 1.4 NA) driven by FluoView software (Olympus, Tokyo, Japan), or with an Ultraview spinning disk confocal imaging system (100× oil 1.4 NA, 60× oil 1.4 NA, or 40× oil 1.3 NA with 1.5× Optovar; PerkinElmer Life and Analytical Sciences, Boston, MA) equipped with a cooled electron multiplying charge-coupled device camera at −50°C (Hamamatsu Photonics K.K., Hamamatsu-shi, Japan) and driven by ImageSuite software, version 3.1 (PerkinElmer Life and Analytical Sciences). Both systems were equipped with a humidified, 5% CO_2 thermoregulated chamber. For quantitative cellular imaging, acquisitions were taken on separate channels using the same parameters (gain and laser power) optimized to keep fluorescent signals in the dynamic range. For confocal image stacks, three-dimensional (3D) and four-dimensional (4D) imaging, confocal z-sections covering the entire depth of the cell were acquired with z-step of 0.5–1.0 μm. Processing and analyses of 3D and 4D image data were performed on Volocity 4 or 5.0 software (Improvision; PerkinElmer Life and Analytical Sciences). When indicated, confocal z-stacks were deconvolved with Volocity 5.0. Subcellular colocalization analyses (object-based analysis, threshold Mander's overlap coefficient, Pearson's coefficient; Bolte and Cordelieres, 2006) and quantitative analyses of organelle dynamic changes (loss of ERC integrity [Horgan *et al.*, 2007], loss of Golgi integrity) are described in Supplemental Data. MetaMorph, version 4.5; Photoshop, version 7.0 (Adobe Systems, Mountain View, CA); and ImageJ 1.41 (National Institute of Health) were used for processing of entire images before cropping to emphasize the main point of the image; processing was limited to background subtraction and brightness/contrast adjustments, unless otherwise indicated.

Statistical Analyses

One-way analyses of variance were used, with p values of <0.05 considered significant (*$p < 0.05$, **$p < 0.01$, and ***$p < 0.001$). Prism 5.0 software (GraphPad Software, San Diego, CA) was used to compare mean values of individual experiments, whereas SAS/STAT 9.1 software (SAS Institute, Cary, NC) was used to compare all single-cell measurements from individual experiments.

RESULTS

Loss of ERC Structural Integrity as a Result of Increased SFK Activity at REs

The death-promoting activity of E4orf4 has been linked to the assembly of a peculiar ring of actin-myosin at the juxtanuclear region requiring the ability of E4orf4 to modulate SFKs and Cdc42-dependent actin polymerization (Robert *et al.*, 2006) (Supplemental Figure S1A, F-actin). The actin structures were shown to be associated with REs exhibiting a striking polarization to the peri-Golgi region where the contractile ring is formed (Supplemental Figure S1A, Rab11a). Based upon this, we have proposed that E4orf4 may perturb RE trafficking as a result of deregulated SFKs and Cdc42 activity, promoting actin remodeling and cell death. Yet, functional links between SFKs, Cdc42, and changes in RE trafficking have not been explored.

As a first step toward this goal, we looked at the effect of E4orf4 on the structural integrity of the ERC in MCF7 or HeLa cells by fluorescent confocal microscopy after cotransfecting them with E4orf4-mRFP and GFP-Rab11a. We reasoned that changes in the morphology of the ERC could reflect alterations in RE trafficking. The ERC consists of an extensive network of tubules that is found predominantly in the pericentrosomal region of MCF7 cells (Figure 1A, Ctl) or more dispersed in the cytoplasm of HeLa cells (see Figure 4A, Tf, Ctl) (Ullrich *et al.*, 1996; Casanova *et al.*, 1999; Wilcke *et al.*, 2000). Confocal image stacks (Figure 1A, grayscale) provided a global view of RE distribution, whereas three-dimensional reconstruction of image stacks (Figure 1A, 3D: green) allowed a better visualization of the tubular morphology of pericentrosomal ERC elements. In both cell lines, E4orf4 induced a loss of pericentrosomal Rab11a associated with fragmentation of Rab11a tubular structures that adopted a dot-like vesicular morphology contrasting with the tubulovesicular organization of REs in control cells (Figure 1A, E4orf4). This phenotype was observed in ~68% of E4orf4-expressing cells compared with ~30% of control cells (Figure 1B) and largely preceded the typical reorganization of the actin cytoskeleton (data not shown). ERC reorganization was also revealed by labeling the transferrin receptor (TfR) that traffics through the ERC (by uptake of fluorescent Tf, or with anti-TfR; data not shown) (Maxfield and McGraw, 2004), indicating that E4orf4 did not simply mislocalize Rab11a. We concluded that the peculiar polarization of REs in response to E4orf4 was preceded by disruption of the ERC.

To determine whether ERC structural changes were linked functionally to SFK signaling, we used characterized E4orf4 mutants defective in their ability to modulate SFKs, SFK inhibitors (PP2, SKI-1), or siRNAs to deplete the three ubiquitously expressed SFKs Src, Yes, and Fyn. Remarkably, E4orf4 mutants unable to interact with SFKs (E4orf4[6R-A]) (Champagne *et al.*, 2004) or displaying Y-F substitutions at tyrosine-phosphorylated motifs (E4orf4[4Y-F]) (Gingras *et al.*, 2002) had no effect on ERC organization (Figure 1B). Furthermore, inhibition of SFKs by using PP2 or SKI-1, or by depletion of Src or Yes, reduced the ability of E4orf4 to perturb ERC organization by ~30–55% (Figure 1B, siSrc, siYes). Under such conditions, Src and Yes were depleted by >80% in both MCF7 and HeLa cells (Figure 1C; data not shown). In marked contrast, control siRNA or siRNA to Fyn had no effect (Figure 1B, siCtl, siFyn), despite the >80% depletion of Fyn (Figure 1C), suggesting a selective requirement for Src and Yes in the context of HeLa and MCF7 cells.

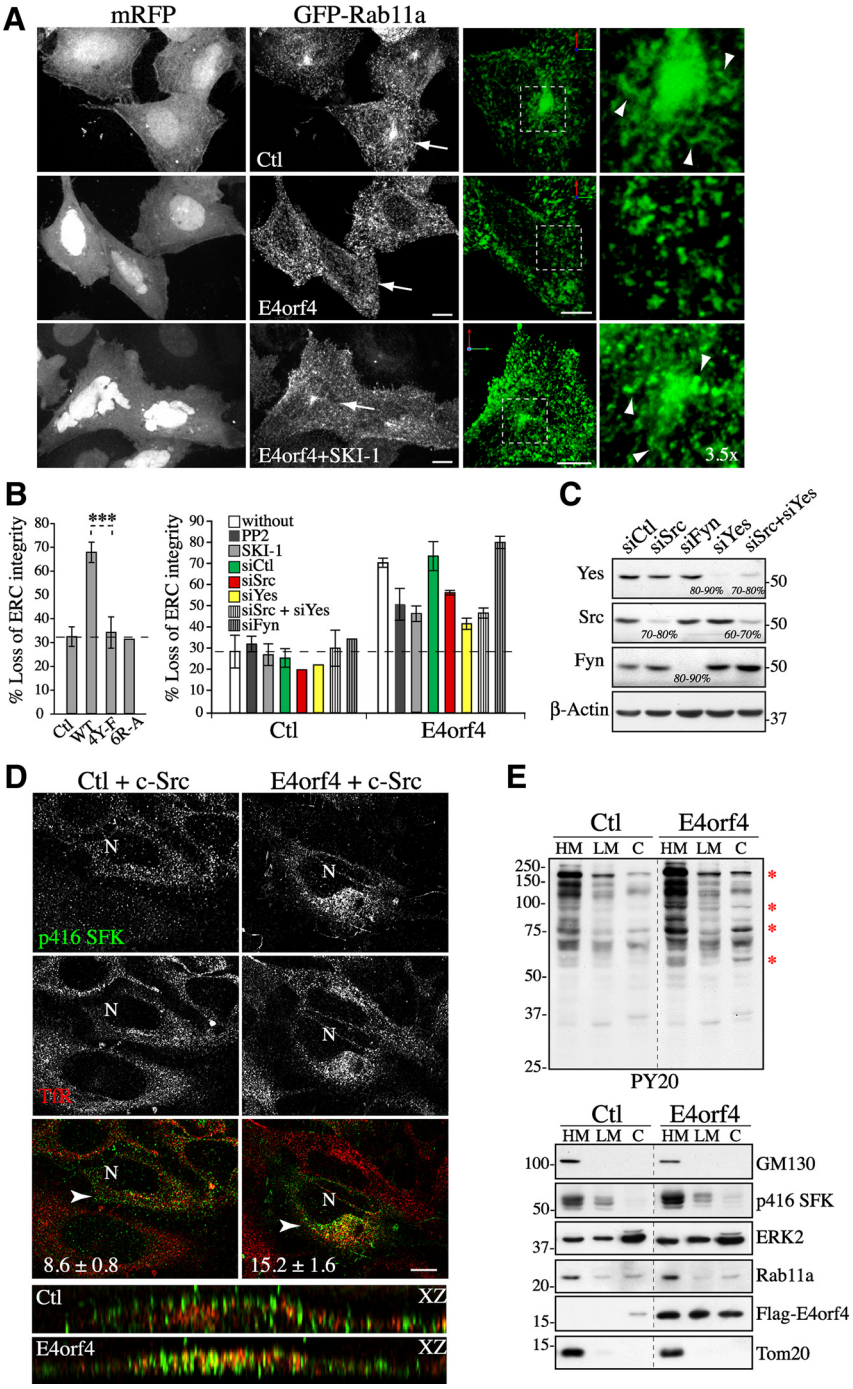

Figure 1. SFK-dependent changes in ERC organization and endosomal SFK signaling in response to E4orf4. (A) Confocal image stacks (grayscale) of MCF7 cells transfected with GFP-Rab11a and mRFP (Ctl) or E4orf4-mRFP, treated or not with SKI-1. 3D reconstructions of images stacks (green, cells designated by arrows) show the tubulovesicular morphology of Rab11a carriers in control cells (arrowheads). Bar, 10 μm. (B) Left, graph depicts the percentages of MCF7 cells showing loss of ERC integrity in response to mRFP (Ctl), or E4orf4 proteins: WT, wild type; 4Y-F, nonphosphorylatable; 6R-A, defective in Src binding. Data are the means ±SD of three experiments, n > 600 cells. Right, graph depicts the percentages of control cells (monomeric red fluorescent protein [mRFP]) or of E4orf4 cells that have been exposed to PP2 or SKI-1 or transfected with the indicated siRNAs, which show ERC dispersal and fragmentation; siCtl, control siRNA. The data are the means ± SD of two experiments performed on MCF7 and HeLa cells, n > 200 cells. Dashed lines delineate the background level of ERC dispersal. (C) Western blots of HeLa extracts harvested 72 h after transfection with siRNAs. The estimated percentages of reduction of SFK protein levels are indicated; β-actin levels: loading controls. (D) Single-plane views from deconvolved z-stacks of HeLa cells expressing Src alone or with FLAG-E4orf4, showing active SFKs (p416 SFK) and TfR staining (REs). The relative percentages of p416 SFKs within TfR-positive endosomes are indicated and were estimated from 3D images by using an object-based analysis function of the Volocity software (described in Supplemental Data); means ±SE, n = 8, $p < 0.01$. Complementary analyses of coincident pixels are available in Supplemental Figure 1B. XZ reconstructions of deconvolved image stacks (arrowhead: *x*-axis). N, nucleus, Bar, 10 μm. (E) Western blots of fractions from control (Ctl) or E4orf4-expressing 293T cells: HM, heavy membranes; LM, light membranes; C, cytosol; anti-phosphotyrosine (PY20), anti-GM130 (*cis*-Golgi), anti-phospho-SFK (p416 SFK), anti-ERK2 (cytosol), anti-Rab11a (REs), anti-FLAG (E4orf4), and anti-Tom20 (mitochondria). Red *, proteins showing E4orf4-induced tyrosine phosphorylation. Dividing lines indicate grouping of images from parts of the same gel.

Based on these data, we reasoned that changes in ERC organization could occur as a consequence of the ability of E4orf4 to divert SFK-dependent signaling to REs. To determine whether this was so, we examined the cellular distribution of phospho-Src in cells expressing equivalent levels of transfected Src, in the presence or absence of E4orf4. Catalytically active Src and REs were probed by immunofluorescence with anti-p416 SFK and anti-TfR, respectively, and the relative distribution of phospho-Src at REs was quantified by analysis of deconvolved confocal image stacks. Using a 3D object-based analysis (Bolte and Cordelieres, 2006), we found that E4orf4-expressing cells displaying polarized REs exhibited a ~1.8-fold increase in the percentage of phospho-Src signal that overlapped with TfR-labeled REs compared with control cells (Figure 1D). Consistently, a threshold approach to evaluate pixel colocalization (Costes *et al*., 2004) revealed a 1.8-fold increase in the mean value for Mander's coefficient of phospho-Src over TfR-labeled REs in cells expressing E4orf4 (Supplemental Figure S1B, tM) and the Pearson's index of overall colocalization also showed a significant increase (Supplemental Figure S1B, Rtot, 1.4-fold). Crude cell fractionation further indicated that E4orf4 stimulated protein tyrosine phosphorylation within endomembranes in 293T, a transformed cell line highly sensitive to the SFK-regulated death-promoting activity of E4orf4 (Champagne *et al*., 2004). In agreement with our

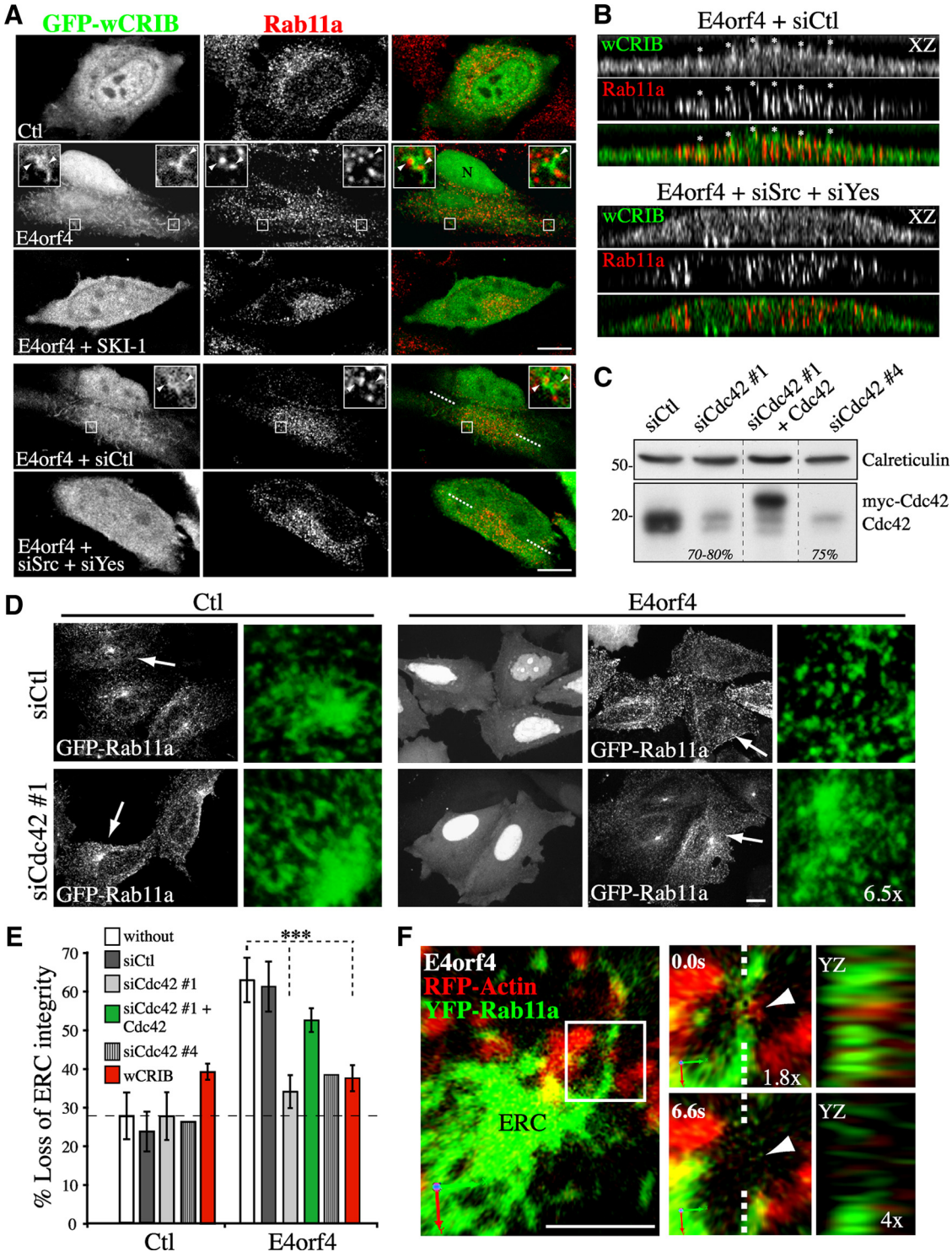

Figure 2. ERC dispersal as a result of SFK-dependent RE-based Cdc42 signaling. (A) Single-plane views of HeLa cells transfected with GFP-wCRIB and mRFP (Ctl) or E4orf4-mRFP, showing tails and puncta of GFP-wCRIB in E4orf4-positive cells associated with REs, as seen by immunostaining of Rab11a, whose formation is abolished by SKI-1 or by depletion of Src and Yes (siSrc+siYes); siCtl, control siRNA. Arrowheads in enlarged images of the boxed regions designate Rab11a endosomes embedded in tail and coat structures labeled by the GFP-wCRIB. (B) XZ reconstructions of deconvolved image stacks showing the overlapping distributions of Rab11a endosomes and tail-like structures labeled by GFP-wCRIB in E4orf4-expressing cells (asterisks). Bar, 10 μm. (C) Western blots of extracts of MCF7 cells harvested 72 h after transfection with the indicated siRNAs with or without myc-Cdc42. The estimated percentages of reduction of Cdc42 protein levels are indicated; calreticulin levels: loading controls. Dividing lines indicate grouping of images from parts of the same gel. (D) Confocal image stacks (grayscale) of MCF7 cells transfected with GFP-Rab11a and mRFP (Ctl) or E4orf4-mRFP, after transfection with the indicated siRNAs. Cells indicated by arrows are shown in high-magnification 3D reconstructions of image stacks (green). Bar, 10 μm. (E) Graph depicting the percentages of mRFP (Ctl) or E4orf4-mRFP–expressing cells, which have been transfected with the indicated siRNAs or with GFP-wCRIB, which show loss of ERC integrity; means ± SD of at least three experiments, n > 300 cells. (F) 3D reconstruction of image stacks of a HeLa

previous findings, the modest increase in phospho-SFKs in response to E4orf4 (Figure 1E, p416 SFK) was associated with a clear change in the tyrosine phosphorylation pattern of cellular proteins (Figure 1E, PY20, asterisks), which we have shown to rely on SFKs (Lavoie *et al*., 2000; Champagne *et al*., 2004). However, proteins that showed a major increase in phosphorylation were largely recovered in a fraction enriched in Rab11a endosomes (Figure 1E, heavy membranes [HM], PY20), whereas little change was observed in the profile of tyrosine-phosphorylated proteins recovered in the light membrane (LM) fraction (Figure 1E, LM). Increased endosomal Src signaling in response to E4orf4 was further corroborated by a more refined cell fractionation protocol that showed higher levels of endogenous phospho-Src associated with Rab11a-enriched membranes relative to TGN membranes (golgin-97) in cells expressing E4orf4 (see Figure 5E). Hence, the data were consistent with a role for endosomal SFK signaling in ERC disruption.

ERC Disruption by Cdc42-mediated Actin Polymerization Downstream of SFKs

Given that the activity of both SFKs and Cdc42 is required for actin remodeling and that Cdc42 mediates the assembly of RE-associated actin particles in response to E4orf4 (Lavoie *et al*., 2000; Robert *et al*., 2006), we sought to address whether SFK signaling could regulate Cdc42 activation at REs. We used the Cdc42/Rac interactive binding (CRIB) domain of N-Wasp fused to GFP (GFP-wCRIB) to probe Cdc42 activation in cells treated with SKI-1 or transfected with a combination of siRNA to Src and Yes, as we did to confirm Cdc42 activation by E4orf4 in situ previously (Robert *et al*., 2006). When expressed at a moderate level GFP-wCRIB serves as a reporter probe for active Cdc42, whereas at high levels it blocks Cdc42 signaling to the actin polymerization machinery (Moreau *et al*., 2000; Scaplehorn *et al*., 2002). In E4orf4-expressing cells, we observed the accumulation of robust GFP-wCRIB–labeled tails and coats in the vicinity of Rab11a endosomes, which were reminiscent of the actin structures generated by Cdc42 (Figure 2A, insets, arrowheads) and were not labeled by GFP alone (data not shown). XZ reconstructions of deconvolved image stacks revealed a striking overlap between the GFP-wCRIB structures and Rab11a endosomes, reflecting the activation of Cdc42 at REs (Figure 2B, asterisks). In contrast, E4orf4 cells exposed to SKI-1 or transfected with siRNAs to Src and Yes displayed a more uniform distribution of GFP-wCRIB just like that seen in control cells, with no significant increased accumulation to Rab11a endosomes (Figure 2, A and B). Because we observed that E4orf4 also localized within some of the GFP-wCRIB structures (Supplemental Figure S1C) and based on our previous findings of a physical interaction between E4orf4 and SFKs (Lavoie *et al*., 2000; Champagne *et al*., 2004), we concluded that a local association between E4orf4 and SFKs at REs could promote Cdc42 activation and actin assembly.

To next determine whether Cdc42 could contribute to the SFK-dependent changes in ERC organization, we used siRNA sequences that achieved >75% depletion of Cdc42 in both MCF7 and HeLa cells (Figure 2C, siCdc42 #1 and #4), or we overexpressed GFP-wCRIB to inhibit Cdc42 signaling (Robert *et al*., 2006). Remarkably, the siRNAs to Cdc42, but not control siRNAs (siCtl), almost ablated E4orf4-induced ERC disruption, just as overexpression of GFP-wCRIB (Figure 2, D and E). Rescue experiments with a siRNA-resistant Cdc42 cDNA ruled out off-target effects (Figure 2, C and E, siCdc42#1+Cdc42). In contrast, depletion of RhoA or inhibition of Rac1 that were also involved in E4orf4-induced actin remodeling and cell death (Robert *et al*., 2006) had no effect on ERC disruption (Supplemental Figure S1, D and E), supporting a specific role for Cdc42 signaling at REs.

To then examine the relationship between Cdc42-mediated actin assembly and fragmentation of REs in response to E4orf4, we performed 4D analyses to follow the dynamic behavior of actin and REs in cells transfected with E4orf4, RFP-actin, and yellow fluorescent protein (YFP)-Rab11a, by using spinning disk confocal microscopy (SDCM). RE remodeling was a very dynamic process and hardly experimentally tractable; nonetheless as seen in the 3D-time sequence in Figure 2F, we repeatedly observed the occurrence of interactions between RFP-tagged actin puncta and Rab11a tubular structures rapidly followed by fragmentation of the tubules. We concluded that actin assembly as a result of E4orf4-mediated SFK and Cdc42 signaling at REs could contribute to ERC disruption, possibly by promoting the scission of Rab11a-positive carriers.

Changes in RE Trafficking Contribute to the Progression of E4orf4-mediated Cell Death

Changes in Rab11 activity influence ERC organization, because overexpression of Rab11 mutants can exacerbate or decrease the tubular morphology of ERC elements (Wilcke *et al*., 2000). Therefore, ERC structural changes as a consequence of SFK-Cdc42–dependent signaling could reflect alteration of Rab11 endosomal traffic that would drive the massive recruitment of REs associated with E4orf4-induced actin remodeling and cell death (Supplemental Figure S1A). To determine whether changes in RE trafficking could contribute to the death-promoting activity of E4orf4, we first used RNA interference for depleting the ubiquitously expressed Rab11 isoform Rab11a (Sakurada *et al*., 1991). HeLa cells were transfected with a previously characterized Rab11a-specific siRNA (siRab11a #1) (Wilson *et al*., 2005) or with a smart pool of siRNAs to Rab11a (siRab11a #2) that both achieved >80% depletion (Figure 3A). The siRNAs to Rab11a, but not control siRNA, reduced the number of E4orf4-expressing cells exhibiting the perinuclear actin network (Figure 3, B and C) and nuclear condensation (Figure 3D) by ~55–65%. The progressive caspase-independent loss of mitochondrial transmembrane potential associated with E4orf4 expression (Lavoie *et al*., 1998) was similarly impaired by Rab11a depletion (Figure 3E, $\Delta\Psi$m). We were unable to measure long-term cell survival under these conditions, because the depletion of Rab11a led to a marked loss of clonogenic survival (>50% inhibition in MCF7 and 293T cells; data not shown). Nonetheless, cell fractionation revealed that E4orf4 increased the association of Rab11a with cellular membranes (Figure 3F). Because membrane insertion of Rabs is coupled to GDP-GTP exchange (Grosshans *et al*., 2006), the results were consistent with a functional role for Rab11a-regulated membrane trafficking in the progression of cell death.

We next sought to measure the transport of protein cargos from the ERC to target compartments to determine the effect of E4orf4 on RE trafficking. Rab11 has been shown to mediate the recycling of internalized protein cargos from the ERC

Figure 2 (cont). cell transfected with FLAG-E4orf4, RFP-actin, and YFP-Rab11a. Confocal z-sections were taken at 6.6-s intervals. Enlarged images of the boxed region show the dynamic association of actin with Rab11a tubular RE followed by scission of the tubule at that site (arrowhead). YZ-views show the spatial superposition of RFP-actin and YFP-Rab11a (dashed lines: *y*-axis). Bar, 5 μm.

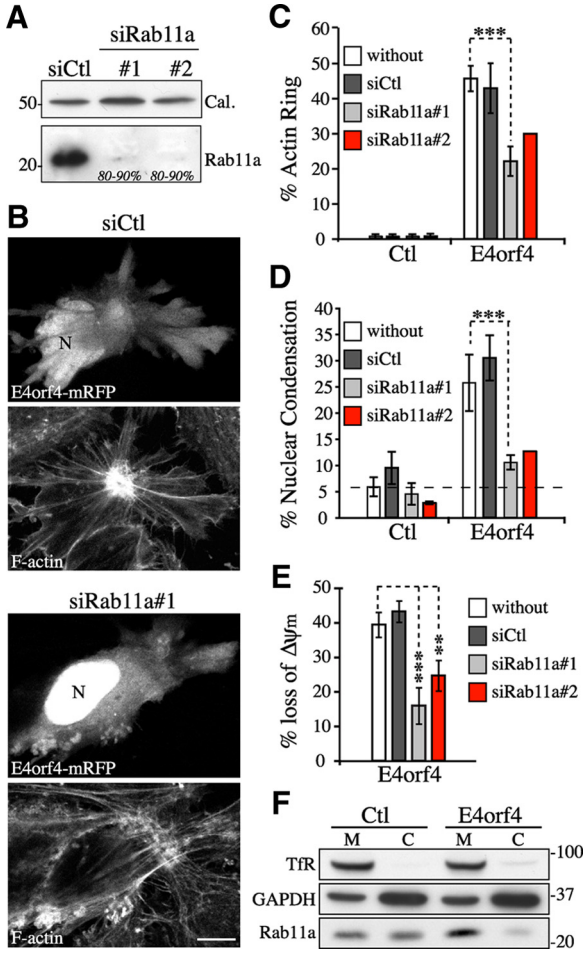

Figure 3. Rab11a membrane trafficking contributes to the progression of E4orf4-induced cell death. (A) Western blots of extracts from HeLa cells transfected with control siRNA (siCtl) or Rab11a siRNAs (siRab11a #1 or #2). Estimated percentages of reduction of Rab11a protein levels are indicated; calreticulin levels: loading controls. (B–E) Analyses of actin remodeling (F-actin staining with phalloidin), nuclear condensation (DNA staining with Hoechst), and ΔΨm (MitoTracker Deep Red) in HeLa cells transfected with the indicated siRNAs before transfection with mRFP (Ctl) or E4orf4-mRFP. (B) Single-plane views of F-actin phenotypes. Bar, 10 μm; N, nucleus. Graphs depict the percentages of control or E4orf4-positive cells showing a juxtanuclear actin ring (C) or nuclear shrinkage and chromatin condensation (D); means ± SD of three experiments for siCtl and siRab11a#1 ($n \geq 425$ cells) and two experiments for siRab11a#2 ($n \geq 230$ cells). The dashed line delineates the background level of nuclear condensation. (E) The graph shows the ratios in percent between the average $\Delta\psi$m/per cell of E4orf4-expressing cells over the average $\Delta\psi$m/cell of E4orf4-negative cells, means ± SE were calculated from 10 cells from a representative experiment. (F) Western blots of membrane (M) and cytosolic (C) fractions isolated from 293T cells transfected with the vector (Ctl) or with FLAG-E4orf4. TfR and glyceraldehyde-3-phosphate dehydrogenase (GAPDH) levels are shown as loading controls for M and C fractions, respectively. A reproducible ~1.5- to 2.0-fold increase in the M/C ratio of Rab11a was observed in E4orf4-expressing cells.

to the plasma membrane and to regulating a direct retrograde transport pathway between EE/RE and the TGN (Ullrich *et al.*, 1996; Wilcke *et al.*, 2000; Maxfield and McGraw, 2004). To examine whether E4orf4 could perturb the recycling of protein cargos back to the plasma membrane, cells were incubated with fluorophore-labeled Tf or with antibody to MHCI to load the endosomal compartment and recycling was measured by comparing the emptying of the Tf or MHCI internal pools within cells after a 30-min chase period. Under such conditions, between 90 and 60% of internalized Tf and MHCI were recycled in control HeLa cells (Figure 4, A and B) (Weigert and Donaldson, 2005), but cells expressing E4orf4 were markedly impaired in recycling of both TfR and MHCI. Indeed, recycling was decreased to ~50% of the recycling exhibited by control cells, whereas the amounts of internalized cargos were not significantly affected (Figure 4, A and B). In contrast, it was found that E4orf4 stimulated EE/RE-to-TGN transport of STxB, an exogenous cargo protein that is transported to the ER by way of the TGN/Golgi membranes (Wilcke *et al.*, 2000; Johannes and Popoff, 2008). In agreement with previous studies (Mallard *et al.*, 1998), control cells exhibited ~15% of total cell-associated STxB-specific labeling concentrated in the TGN after 20 min of internalization at 37°C (Figure 4C). In the early stages of E4orf4 expression, however, the fraction of TGN-associated STxB was reproducibly increased by 1.5-fold, suggesting that RE-to-TGN membrane transport was enhanced.

Golgi Remodeling as a Result of Cdc42-regulated Transport of REs to the Golgi Complex

So far, the data argued that changes in RE trafficking could be coupled to death signaling via alteration of Golgi dynamics, given that RE-to-TGN membrane transport has been linked to the structural integrity of the Golgi (Derby *et al.*, 2007), which in turn has been involved in stress sensing and cell death (Hicks and Machamer, 2005). To investigate this possibility, we first performed 4D analyses using SDCM to track the dynamic behavior of REs and the relationship to Golgi membranes in cells transfected with Rab11a-YFP (RE) and GalT-mRFP (*medial-trans*-Golgi) in the presence or absence of E4orf4. 3D-time sequences revealed that Rab11a vesicles interacted dynamically with Golgi membranes, showing transient contacts followed by the disappearance of Rab11a staining, which was presumably diluted upon membrane fusion (Figure 5A, arrowheads in frames 1:10–1:40; and Supplemental Video 1). Although such interactions were observed in control cells, they were increased by approximately twofold in E4orf4-expressing cells (Figure 5, A and B), corroborating an enhanced transport of STxB to the TGN in response to E4orf4. RE–Golgi interactions often coincided with stretching and fission of Golgi elements at those sites, and in E4orf4-expressing cells the incidence of RE–Golgi interactions that were followed by fission of Golgi elements was increased by ~2.5-fold (Figure 5A, frames 1:50, 2:00; and C; and Supplemental Video 1). RE–Golgi membrane interactions were not stochastic; instead, several cycles of interactions occurred at the same site and likely reflected a regulated membrane mixing process affecting Golgi dynamics (Supplemental Figure S2A). We further observed that membrane fission was taking place concomitantly with the emergence of actin structures (Supplemental Figure S2B and Supplemental Video 2), suggesting that RE-mediated delivery of actin remodeling factors could promote Golgi membrane fission. An increase in RE–Golgi interactions was also observed by labeling REs with fluorescent Tf, which was correlated with a 2.2-fold increase in the localization of Tf to the Golgi (tM) (Figure 5, B and D). Since Tf is not normally transported to the Golgi complex with high efficiency, E4orf4 seemed to mobilize REs to the Golgi, thereby perturbing both Golgi membrane dynamics and recycling of cargos to the plasma membrane. Importantly, depletion of Cdc42 impaired E4orf4-induced RE–

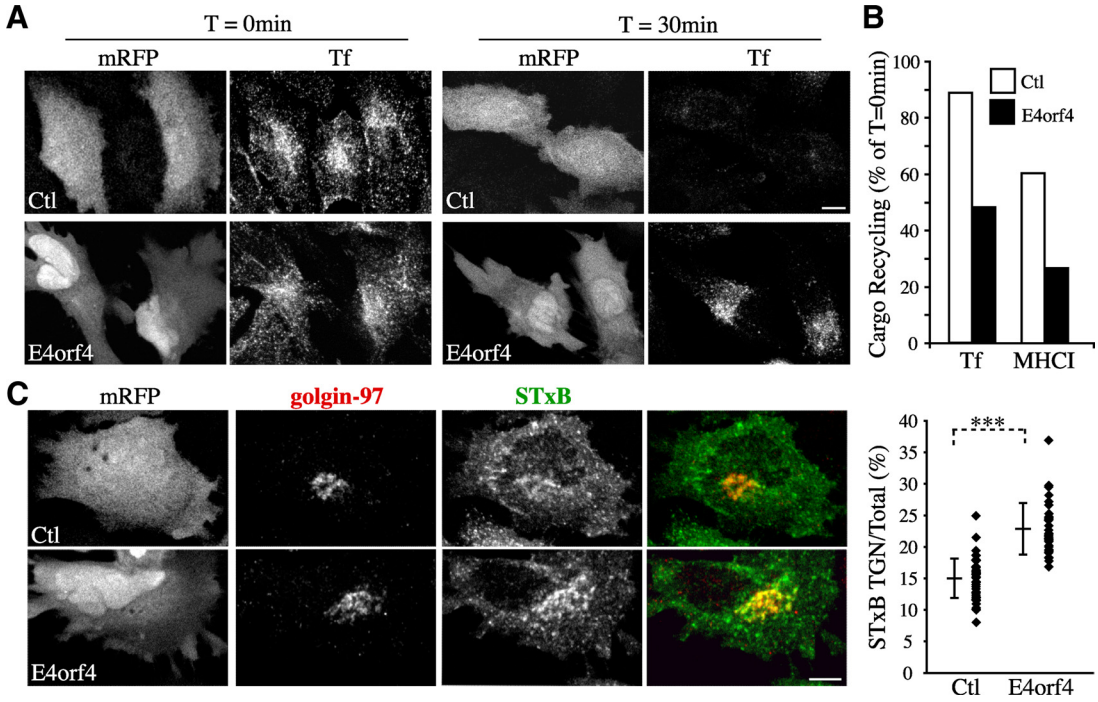

Figure 4. E4orf4 impairs the recycling of protein cargos back to the plasma membrane, whereas it stimulates endosome-to-TGN transport of STxB. (A) Confocal image stacks of HeLa cells transfected with mRFP (Ctl) or E4orf4-mRFP showing internalized Alexa-488–labeled-Tf after 30 min at 37°C (T = 0 min), compared with the remaining internal pool after a 30-min chase at 37°C (T = 30 min). (B) Recycling of internalized Alexa-488–labeled-Tf or of MHCI (after loading cells with antibody to MHCI) was measured by comparing the emptying of protein cargos internal pools within cells after a 30-min chase by quantitative fluorescence analyses of image stacks. Data are the means calculated from ≥10 cells from a representative experiment. (C) Confocal image stacks of HeLa cells transfected with mRFP (Ctl) or E4orf4-mRFP incubated with Alexa-488–conjugated-STxB for 20 min at 37°C, which show internalized STxB reaching the TGN revealed by immunostaining of golgin-97. The graph shows ratios in percent between total fluorescence intensity in the TGN area over whole cell total fluorescent contents; means ± SD of three experiments, n ≥ 34 cells. Bars, 10 μm.

Golgi membrane interactions (Figure 5, B and C), just as it prevented ERC fragmentation and presumably the changes in RE trafficking in response to E4orf4 (Figure 2, D and E). However, Cdc42 depletion did not affect RE-Golgi associations occurring at low frequency in control cells, suggesting that Cdc42 could control a retrograde pathway for the mobilization of REs in response to cell rearrangement that was stimulated by E4orf4-SFK signaling.

To further analyze the impact of E4orf4 on the distribution of REs and Golgi membranes, PNSs were fractionated using a self-generated Opti-Prep gradient. In control cells, RE markers (Rab11a, TfR) were enriched in low density fractions (peak 1), whereas Golgi markers were found either in high-density fractions (golgin-97, TGN marker, peak 2) or distributed between both (GM130, *cis*-Golgi marker) (Figure 5E). Remarkably, E4orf4 induced the scrambling of REs and Golgi membranes, as reflected by the codistribution of TfR, Rab11a, and GM130 in a peak of intermediate density fractions (Figure 5E, red dashed lines). The phosphorylation/activation of SFKs was selectively elevated in intermixed membranes (Figure 5E, p416 SFKs), whereas little change in the levels of Src and Yes was detected, further suggesting that endosomal SFK signaling could regulate the transport of REs to the Golgi. Significant levels of E4orf4 were also detected within intermixed membranes (Figure 5E, FLAG-E4orf4), corroborating colocalization analyses (Supplemental Figure S1C) and supporting an E4orf4 endosomal activity. Thus these results were consistent with those of cell imaging, and further suggested that the polarization of RE traffic to the Golgi induced Golgi membrane remodeling.

RE-mediated Loss of Golgi Integrity Contributes to the Progression of Cell Death

The above-mentioned data suggested that an increase in RE-to-Golgi membrane transport could perturb Golgi structural integrity. Actually, >55% of MCF7 or HeLa cells expressing E4orf4 exhibited scattering of both *cis*- and *trans*-Golgi membranes (Figure 6A, arrows 2; and D), whereas >80% of control cells showed a typical compact juxtanuclear staining of Golgi membranes (Figure 6A, arrowheads 1; and D). The Golgi fragments contained both *cis*- and *trans*-markers, suggesting that E4orf4 induced the disjoining of the Golgi ribbon (Supplemental Figure S3A). Golgi membrane scattering occurred after ERC fragmentation (Figure 6B) but before nuclear condensation (Supplemental Figure S3B). Notably, the wide-spectrum caspase inhibitors zVAD-FMK and QVD-OPh had no impact on the extent or the incidence of Golgi fragmentation (Supplemental Figure S3B), despite their efficient inhibition of caspases in response to STS (Supplemental Figure S5C). The use of both zVAD-FMK and QVD-OPh to determine the caspase dependency has been validated both in vitro and in vivo, because the latter is a potent inhibitor of caspase-2 and -6 (Chauvier *et al.*, 2007). Thus, we concluded that loss of Golgi integrity in response to E4orf4 was a caspase-independent event, in agreement with previous work showing the absence of active caspases in most cancer cell lines expressing E4orf4 (Lavoie *et al.*, 1998; Robert *et al.*, 2002; Li *et al.*, 2009).

We further found that Golgi membrane scattering was associated with a defect in the transport of nascent proteins

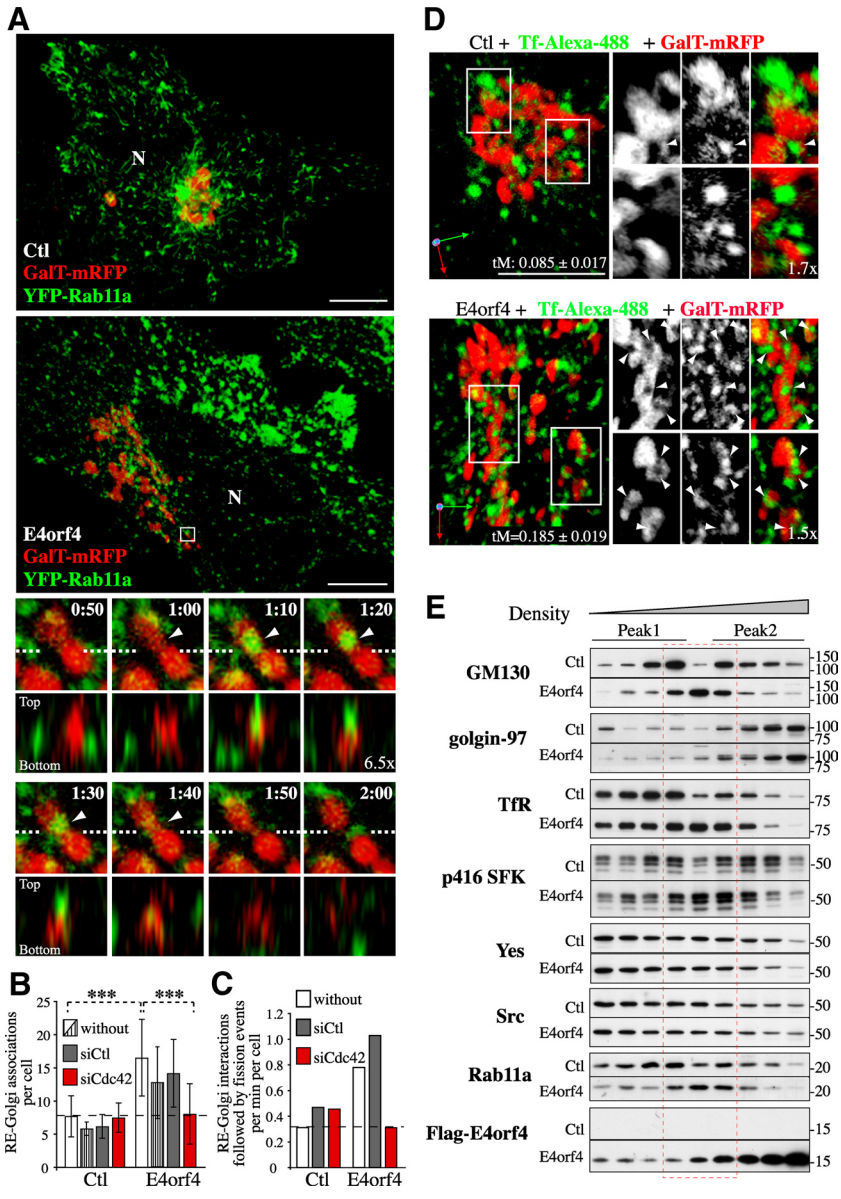

Figure 5. Remodeling of Golgi membranes by Cdc42-mediated increase in RE-to-Golgi membrane transport and scrambling of RE–Golgi membranes. (A) 3D reconstructions of image stacks of HeLa cells transfected with the vector only (Ctl) or with FLAG-E4orf4 together with β-1,4-galactosyl transferase (GalT)-mRFP and YFP-Rab11a. E4orf4 cells exhibiting ERC fragmentation were selected for 4D analyses. Enlarged images of the boxed region show a representative 3D-time sequence from confocal z-sections taken at ≥10-s intervals (Supplemental Video 1). XZ views show the spatial superposition of YFP-Rab11a-RE and GalT-mRFP-Golgi tubules and mixing of membrane markers (arrowheads in frames 1:10–1:40) followed by fragmentation of the Golgi element (frames 1:50, 1:60); dashed lines: *x*-axis. N, nucleus; Bars, 10 μm. (B) The average number of RE–Golgi membrane associations per cell were determined from analyses of 3D reconstructions of image stacks of HeLa cells transfected with the indicated siRNAs before transfection with the vector only (Ctl), or with FLAG-E4orf4 together with GalT-mRFP and YFP-Rab11a (open bars); RE were also visualized with Tf-Alexa-488 (striped bars). Data are the means ± SD from three experiments using YFP-Rab11a, n ≥ 14 cells and of six or more cells by using Tf-Alexa-488. (C) The average incidence of RE–Golgi interactions followed by fission of the Golgi element was determined from 3D sequences; means ± SD from five or more cells. Dashed lines delineate the average incidence of RE–Golgi membrane associations (B) or of RE-Golgi dynamic interactions followed by Golgi fission (C) in control cells. (D) 3D reconstructions of image stacks of HeLa cells transfected with GalT-mRFP and the vector only (Ctl) or FLAG-E4orf4. REs were visualized after a 45-min uptake assay with Tf-Alexa-488 and confocal z-sections were acquired for no >15 additional minutes. Enlarged images of the boxed regions show Tf-positive carriers embedded in Golgi membranes, seen at a higher frequency in E4orf4 cells (arrowheads). Threshold-adjusted Mander's coefficients (tM) of Tf over GalT are indicated; means ± SE calculated from six or more cells from a representative experiment. Bars, 10 μm. (E) PNS from 293T cells transfected with the vector (Ctl) or FLAG-E4orf4 were fractionated using a linear 10–20-30% Opti-Prep gradient. Fractions (equal volumes) were analyzed by Western blot using the indicated markers; Peak 1, low-density fractions; peak 2, high-density fractions; red dashed lines, intermediate density fractions composed of mixed RE and Golgi membranes in E4orf4 cells.

from the Golgi. This was revealed using VSVG-ts-GFP as protein cargo, which was retained in the ER at the restrictive temperature (39.5°C) and transported through the Golgi upon shifting to a permissive temperature (31.5°C) (Supplemental Figure S3C). Although VSVG-ts-GFP reached the plasma membrane by 30 min in control cells, it was still retained in Golgi fragments in E4orf4-expressing cells showing scattered Golgi membranes (Supplemental Figure S3C). This looked like a block in protein exit from the Golgi because by 3 h, there was a 1.8–3.0-fold increase in VSVG protein accumulating in the perinuclear region (Figure 6C). Under such conditions, E4orf4 had little impact on ER–Golgi protein transport kinetics or on the retrograde transport of proteins between the Golgi and ER, as suggested by the effect of brefeldin A, a drug inducing the resorption of Golgi membranes into the ER (Doms *et al.*, 1989; Lippincott-Schwartz *et al.*, 1990) (Supplemental Figure S3, C and D). This suggested that normal Golgi to plasma membrane protein transport was interrupted as a result of the changes in Golgi membrane dynamics induced by deregulated RE trafficking.

We next attempted to confirm the functional relationship between alterations of RE trafficking and Golgi dynamic changes by interfering with SFK or Cdc42 signaling so as to prevent the polarization of RE traffic. Consistent with their lack of effect on the ERC, E4orf4 mutants unable to modulate SFKs were incapable of inducing efficient Golgi membrane scattering (Figure 6D). Furthermore, inhibition of SFK activities or depletion of Src or Yes, but not Fyn, reduced E4orf4-dependent Golgi disassembly by ~50–70% (Figure 6, E and F) just like depletion of Rab11a (~55–80% inhibition) (Figure 6, E and G), depletion of Cdc42 (~80% inhibition) (Figure 6, E and G), or inhibition of actin polymerization using a low concentration of LatA (Figure 6G). Under such condition, no

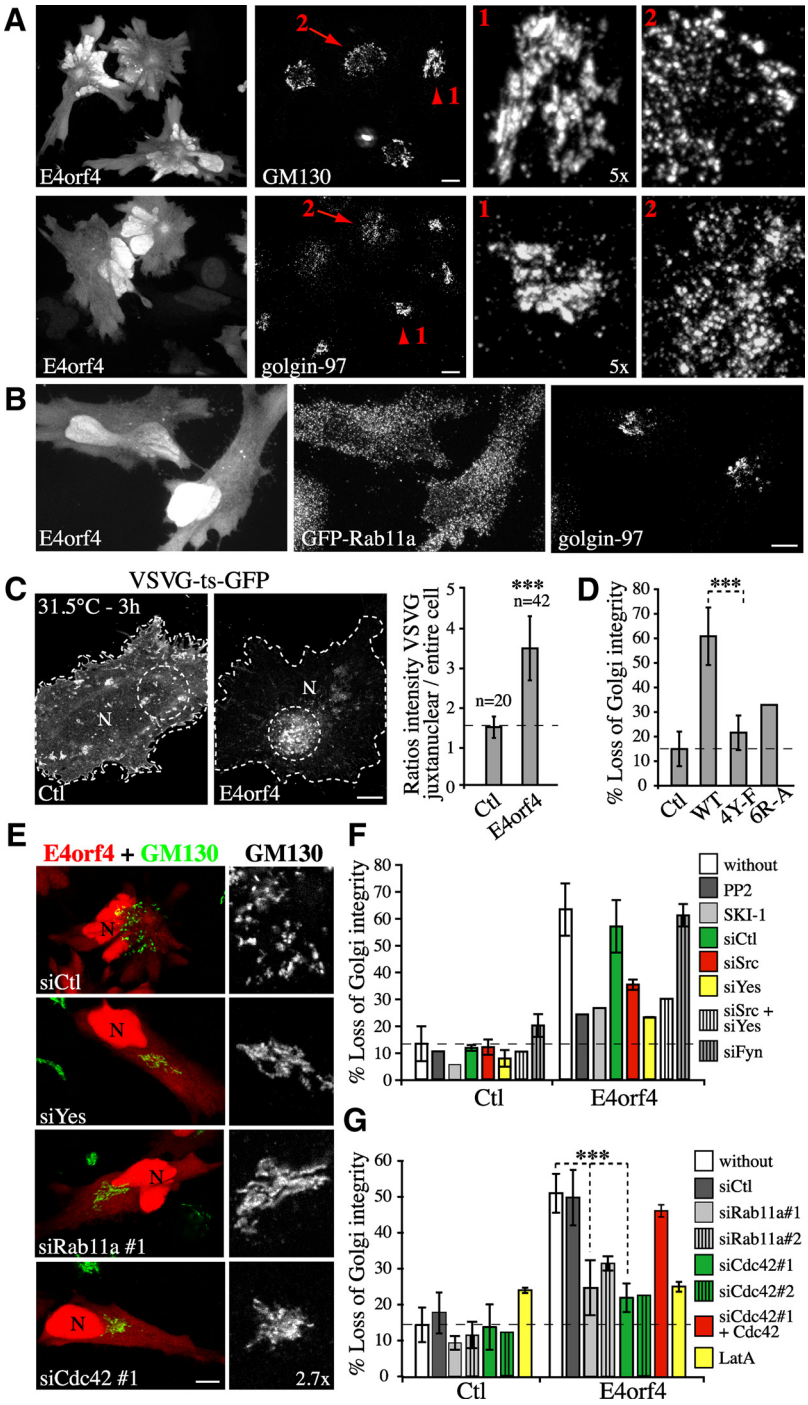

Figure 6. Loss of Golgi integrity via a pathway involving SFKs, Cdc42, actin, and Rab11a membrane trafficking (A) Confocal image stacks of HeLa cells transfected with E4orf4-mRFP, showing staining of *cis*-Golgi (GM130 staining) and TGN (golgin-97 staining). Arrowheads and arrows designate staining patterns in control (high magnifications, marked 1) and in E4orf4 cells (high magnifications, marked 2). Bars, 10 μm. (B) Image stacks of HeLa cells transfected with E4orf4-mRFP and GFP-Rab11a, showing ERC fragmentation and incomplete Golgi disassembly (golgin-97). Bar, 10 μm. (C) Single-plane views of HeLa cells expressing VSVG-ts-GFP and mRFP (Ctl) or E4orf4-mRFP, shifted to 31.5°C for 3 h in the presence of cycloheximide; N, nucleus; Bar, 10 μm. Graph shows the ratios of the average intensity of VSVG protein in the juxtanuclear region over that in the entire cell; means ± SD of three experiments. (D) Graph depicts the percentages of HeLa cells transfected with mRFP (Ctl) or the indicated E4orf4 constructs which show loss of Golgi integrity; means ± SD of three experiments, n > 360 cells. (E–G) HeLa cells were transfected with mRFP (Ctl) or E4orf4-mRFP after transfection with the indicated siRNAs, or in the presence of SFK inhibitors (PP2, SKI-1) or LatA. (E) Single-plane views showing protection of Golgi integrity (GM130 staining) by depletion of Yes, Cdc42, or Rab11a; N nucleus, Bar, 10 μm. (F–G) Graphs depicting the percentages of cells displaying scattered Golgi membranes; means ± SD of two experiments (siSrc, siYes, siFyn, siRab11a#2, and LatA, n ≥ 200 cells) and five experiments (siCtl, siCdc42#1 and siRab11a#1, n ≥ 450 cells). Dashed line delineates the background level of Golgi membrane scattering.

gross disruption of the actin cytoskeleton or the Golgi was observed in control cells (Supplemental Figure S4A), supporting a role for actin dynamics per se that relied on Cdc42, but no on RhoA or Rac1 (Supplemental Figure S4B).

We then sought to explore the functional relevance of Golgi membrane scattering by using RNA interference to deplete syntaxin 6, a TGN-associated trafficking factor involved in the fusion of EE/RE with Golgi membranes (Johannes and Popoff, 2008). We reasoned that if the scattering of Golgi membranes was relying in part on retrograde transport to the TGN, depletion of syntaxin 6 should prevent loss of Golgi integrity by interfering with the outcome of RE–Golgi interactions, without affecting upstream signaling events at the ERC. As predicted, knockdown of syntaxin 6 expression inhibited Golgi fragmentation, but not ERC disruption in E4orf4-expressing cells (Figure 7, A–D, siStx6). Remarkably, in these cells the frequency of nuclear condensation and the loss of mitochondrial transmembrane potential were also inhibited by ~50–70% (Figure 7E). To obtain further support for a role for Golgi dynamics, complementary experiments were designed to examine the effect of Golgi matrix proteins that were associated with Golgi dynamic changes during apoptosis (golgin-160) (Mancini *et al*., 2000; Hicks and Machamer, 2002; Maag *et al*., 2005) or during

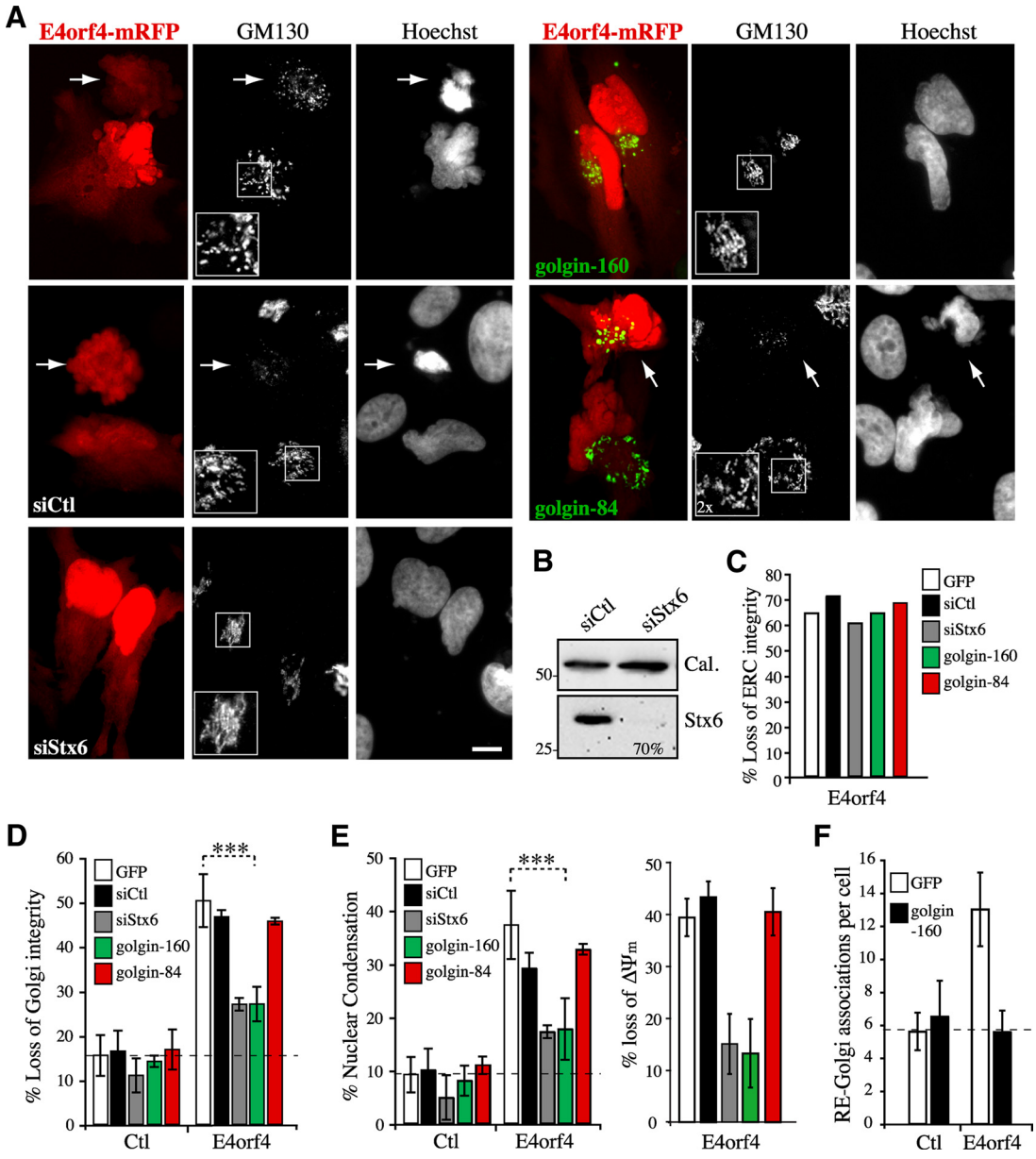

Figure 7. Changes in Golgi membrane dynamics as a result of RE-to-Golgi membrane transport contribute to the progression of E4orf4-induced cell death. HeLa cells were transfected with mRFP (Ctl) or E4orf4-mRFP after transfection with the indicated siRNAs (siCtl, control siRNA; siStx6, syntaxin 6 siRNA), or together with golgin-160-GFP or golgin-84-GFP. (A) Epifluorescence images of E4orf4 cells, showing a marked protection of Golgi structure (GM130 staining) and of nuclear morphology (Hoechst staining) after depletion of syntaxin 6 or in the presence of golgin-160, but not golgin-84. Arrows designate E4orf4-expressing cells displaying typical Golgi membrane scattering associated with nuclear condensation. Bars, 10 μm. (B) Western blots of HeLa extracts harvested 72 h after transfection with siRNAs. The estimated percentage of reduction of syntaxin 6 protein levels is indicated; cal: calreticulin levels are shown as loading controls. (C–E) The mean percentages of cells displaying the indicated phenotypes were calculated from ≥30 cells from a representative experiment (C) or (D and E) from four experiments for golgin-160 ($n > 600$ cells) and two experiments for golgin-84 or siRNAs ($n > 200$ cells) (means ± SD) or from >10 cells from a representative experiment (loss of $\Delta\Psi$m; means ± SE). (F) Graph depicting the number of RE-Golgi membrane associations estimated from 3D reconstructions of image stacks of HeLa cells transfected with YFP-Rab11a and GalT-CFP, together with mRFP (Ctl) or E4orf4-mRFP with GFP or golgin-160-GFP; means ± SD of five or more individual cells. The dashed lines in graphs delineate background levels of Golgi membrane scattering (D), nuclear condensation (E), or RE–Golgi associations (F).

mitosis (golgin-84) (Diao *et al.*, 2003). It was found that a moderate expression of golgin-160 or golgin-84 neither induced Golgi fragmentation in control cells nor affected ERC disruption in response to E4orf4 (Figure 7, C and D). Intriguingly golgin-160, but not golgin-84, reduced the occurrence of Golgi fragmentation and nuclear condensation, as well as the loss of mitochondrial transmembrane potential in E4orf4-expressing cells, to a level similar to that observed in syntaxin 6-depleted cells (Figure 7, A, D, and E). The mechanism by which golgin-160 interfered specifically with E4orf4-induced Golgi membrane scattering is currently unclear, but we observed that it prevented E4orf4-mediated RE-Golgi interactions and presumably membrane fusion (Figure 7F), in agreement with the idea that deregulated

retrograde transport of REs was bound to Golgi fragmentation. Hence, the results suggested that Golgi dynamic changes were not simply a consequence of deregulated RE trafficking, but rather contributed to the death process.

RE-mediated Caspase-independent Golgi Fragmentation and Cell Death in Response to STS

Having identified a novel cross-talk between the ERC and the Golgi during E4orf4-mediated cell death, we attempted to explore its relevance by investigating whether this pathway could regulate other death programs. To do so, we used STS as a prototype apoptotic inducer. We found that Golgi disassembly in response to STS only partially relied on caspases, because caspase inhibitors did not abolish Golgi fragmentation but reduced it by ~50% in MCF7 or HeLa cells exposed to STS for 4 h (Figure 8, A, D, and F; and Supplemental Figure S5, A and B). Under such conditions, the frequency of apoptotic nuclear fragmentation was inhibited by >90% (Supplemental Figure S5A), and caspase activities were efficiently reduced in most cells, especially in the presence of QVD-OPh (Supplemental Figure S5C). We were also unable to detect active caspase-3 in HeLa cells exhibiting Golgi membrane scattering in the presence of QVD-OPh (Supplemental Figure S5D), further indicating that persistent Golgi fragmentation occurred in the absence of efficient activation of effector caspases. These cells exhibited a marked dispersal and fragmentation of ERC elements that strikingly overlapped with scattered Golgi elements (Figure 8A, siCtl QVD+ STS; and C and E), suggesting that like E4orf4, STS triggered the scrambling of REs and Golgi membranes along with disorganization of Golgi membranes. Actually, the retrograde transport of STxB to the TGN was increased by ~2.5-fold (Figure 8B). Remarkably, depletion of Src, Yes or Cdc42 or inhibition of actin dynamics with LatA significantly impaired STS-induced ERC disruption (~50–80% reduction) (Figure 8, A, C, and E; data not shown) and provided a similar protection of Golgi structural integrity (Figure 8, A, D, and F), just like depletion of Rab11a or syntaxin 6 and overexpression of golgin-160 (Figure 8, E and F). Thus, this corroborated our findings using E4orf4 and strongly suggested that SFKs-Cdc42-actin–regulated changes in the traffic of REs could contribute to apoptotic Golgi disassembly.

To obtain further support for a role for SFKs to STS-mediated death signaling, we analyzed the pattern of tyrosine-phosphorylated proteins before and after exposure of cells to STS in the presence of QVD-OPh. As expected, STS reduced the tyrosine phosphorylation of several cellular proteins in both MCF7 and HeLa cells, in line with its activity as a wide-spectrum kinase inhibitor. Nonetheless, some proteins reproducibly displayed selective and persistent phosphorylation in response to STS, in a manner that relied on SFKs (Figure 9A, arrows). This was observed for protein bands with apparent molecular weight similar to those whose tyrosine phosphorylation was induced by E4orf4, notably for ~p200 and ~p90 proteins (Figure 1E, asterisks; and 9A, arrows), suggesting that selective SFK substrates could regulate both E4orf4- and STS-induced cell death through their effect on organelle dynamic changes. In support of this idea, inhibition of SFKs (SU6656) or depletion of Src or Yes reduced STS-induced caspase-independent nuclear condensation by ~30–50%, just like depletion of Cdc42, Rab11a, or syntaxin 6 and overexpression of golgin-160 (Figure 9, B and C).

DISCUSSION

This study conveys two novel and interrelated messages: first, CD signaling induces changes in RE trafficking engaged in the transmission of death signals through a pathway involving SFKs, Cdc42, actin, and Rab11a; second, diversion of RE traffic to the Golgi apparatus promotes the intermixing of RE and Golgi elements and Golgi dynamic changes that contribute to the progression of cell death. These findings were substantiated using two unrelated triggers of caspase-independent CD and are presented in a working model in Figure 10 in which the coordinated actions of SFKs, Cdc42, and Rab11a at REs may define a novel regulatory mechanism whereby actin-regulated membrane trafficking influences cell commitment to death. These findings have important implications in RE trafficking and CD signaling that are discussed below.

Mobilization of the ERC has been reported in many activation processes requiring organelle plasticity and membrane rearrangements (van Ijzendoorn, 2006; Saraste and Goud, 2007), but the mechanisms have remained enigmatic. Here, we obtained strong evidence that the ERC is mobilized in response to death signals through a pathway involving RE-based SFKs and Cdc42 signaling that leads to ERC structural changes reflecting enhanced RE trafficking to the Golgi and decreased recycling of protein cargos back to the plasma membrane. Such a process was found to regulate cell death induced by E4orf4 and by a general apoptotic trigger (STS), providing strong support for a prevalent role. The requirement for Rab11a indicated that alterations of RE trafficking were not simply a consequence of death signaling but rather reflected the activation of a retrograde membrane trafficking pathway controlled by Rab11a. Hence, cell killing induced by E4orf4 could follow its ability to hijack a novel pathway directing the mobilization of an intracellular pool of membranes that could contribute to the changes in organelle dynamics regulating death programs. E4orf4 has been shown to interact with the kinase domain of SFKs and to redirect SFK signaling to a subset of targets involved in actin remodeling (Lavoie *et al*., 2000; Gingras *et al*., 2002; Champagne *et al*., 2004; Robert *et al*., 2006; Smadja-Lamere *et al*., 2008). Here, we found that E4orf4 acts by diverting SFK signaling to REs and promoting RE transport to selected compartments, notably to the Golgi, where they may facilitate the dynamic rearrangement of membranes. Hence, assembly of the peculiar perinuclear actin network in response to E4orf4 is probably the outcome of the polarized traffic of membranes, which might promote a massive delivery of actin-remodeling factors. Whether E4orf4 has evolved the ability to exploit RE trafficking for the purpose of promoting the transport of viral components during adenovirus infection remains to be determined.

The detailed molecular mechanism whereby E4orf4 hijacks RE trafficking remains to be clarified, but could entail E4orf4's ability to associate with lipid raft constituents that traffic through the ERC (unpublished data) in addition to SFK binding and phosphorylation of E4orf4. It is currently unclear why Src and Yes and not Fyn were involved in the retrograde trafficking of REs in the context of HeLa and MCF7 cells. SFKs were found to show distinct modes of spatial activation and membrane delivery that rely partly on endosome subtype requirements (Sandilands *et al*., 2007b). Although we cannot rule out a cell-type–specific contribution of SFKs, Src and Yes could share a common mode of activation in Cdc42-Rab11a–positive endosomes and cellular targets, such as the proteins of ~90 and ~200 kDa whose tyrosine phosphorylation was found here to be stimulated

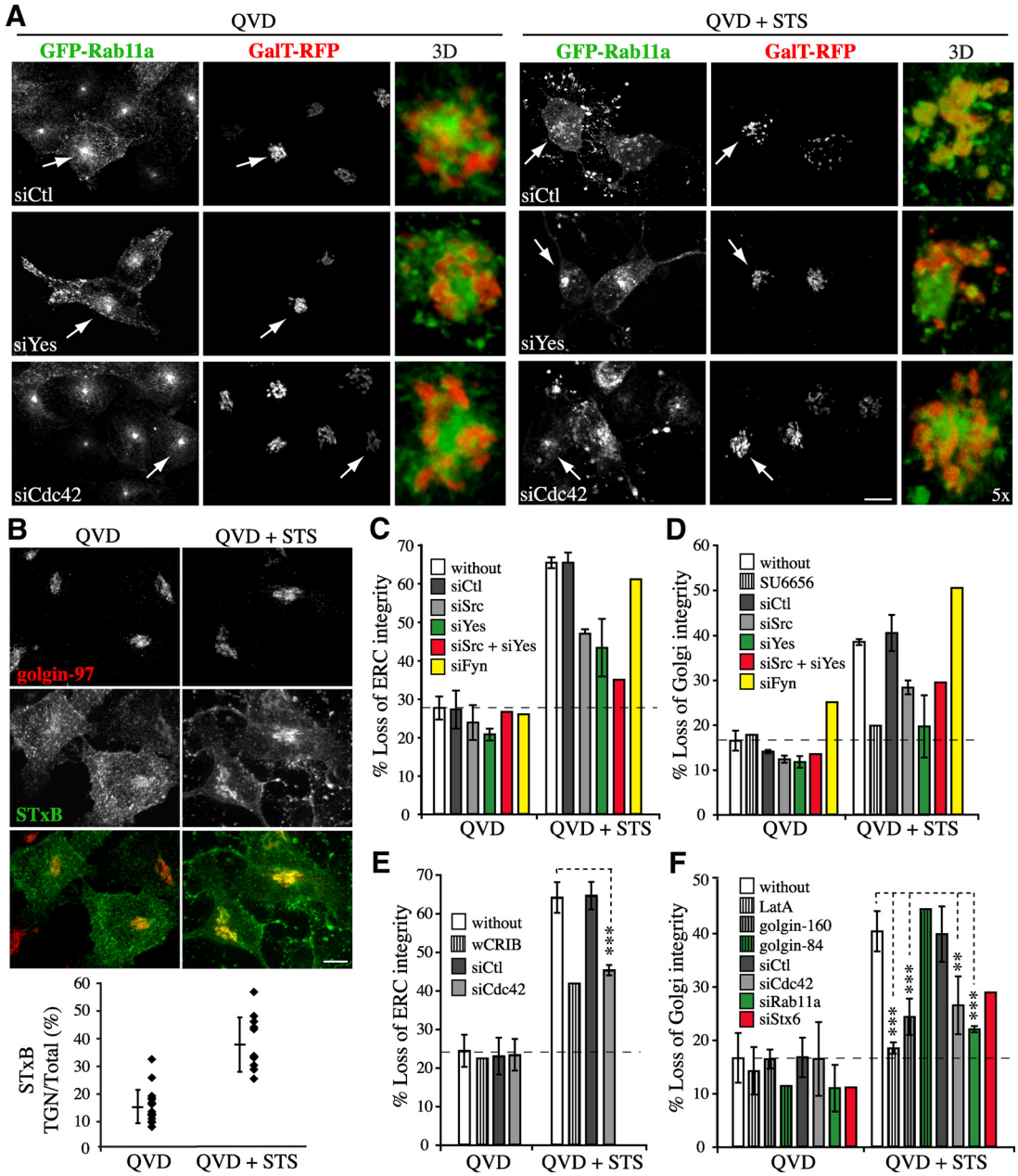

Figure 8. STS-induced caspase-independent fragmentation of the ERC and the Golgi complex involves SFKs, Cdc42, actin, and Rab11a membrane trafficking. (A) Confocal image stacks of MCF7 cells (grayscale) transfected with the indicated siRNAs before transfection with GFP-Rab11a and GalT-mRFP. Cells were exposed to STS for 4 h in the presence of caspase inhibitor (QVD-OPh). Arrows designate the peri-Golgi regions shown in high-magnification 3D reconstructions of image stacks, emphasizing Rab11a and GalT staining patterns. Bar, 10 μm. (B) Confocal image stacks of HeLa cells exposed to STS + QVD-OPh for 4 h and incubated with Alexa-488–conjugated STxB for 20 min at 37°C, which show internalized STxB concentrated in the TGN revealed by immunostaining of golgin-97. The graph shows ratios in percent between total fluorescence intensity in the TGN area over whole cell total fluorescent contents; means ± SD were calculated from a representative experiment, n ≥ 11 cells. Bar, 10 μm. (C–F) Graphs depicting the percentages of QVD (Ctl) and of STS + QVD-treated MCF7 and HeLa cells transfected with the indicated siRNAs, GFP-wCRIB, golgin-160-GFP, or with golgin-84-GFP or pretreated for 1 h with the indicated drugs that displayed fragmentation of the ERC (C and E) or Golgi disassembly (D and F). Data are the means ± SD of two experiments, n > 200 cells (C and D) or three experiments, n > 340 cells (E and F) except for siStx6, golgin-160, and golgin-84, whose means were calculated from >100 cells from one experiment. Dashed lines delineate background levels of ERC or Golgi fragmentation.

by E4orf4 and STS. Regardless of the mechanism, our findings further highlight the emerging function of SFKs in endosomal trafficking, which has been linked with various Rho proteins and with the actin-dependent transport of Rab11-endosomes to the peripheral membrane (Sandilands *et al*., 2004, 2007a; Sandilands and Frame, 2008). Here, we provided strong evidence that SFKs control the activation of Cdc42 at REs, which in turn regulates the local actin assembly stimulating the transport of REs from the ERC to the Golgi complex. Besides the likely contribution of actin to the budding and fission of ERC-derived membrane carriers (Figure 10) (Lanzetti, 2007), the polarity function of Cdc42

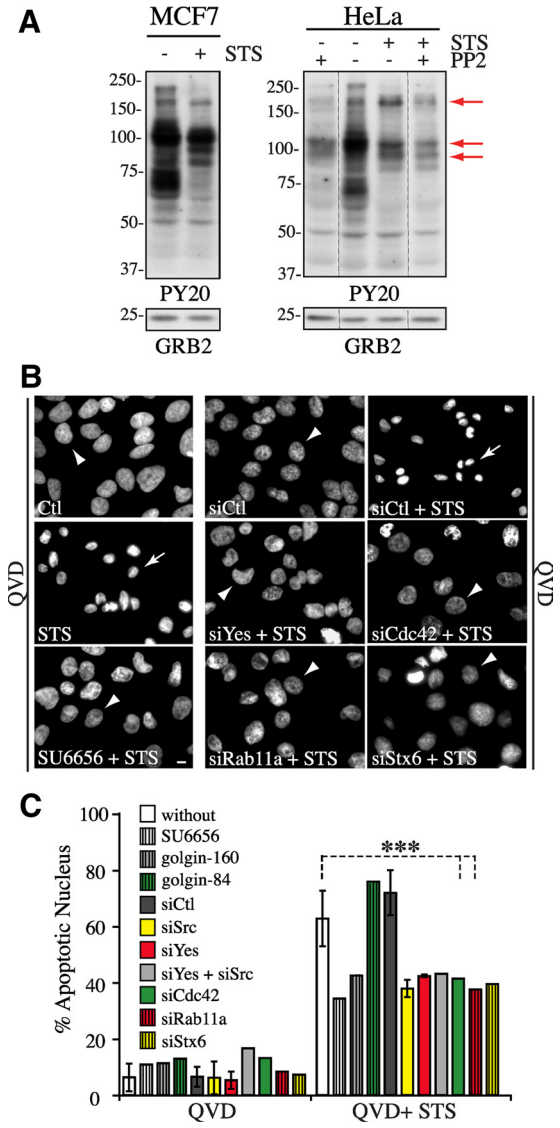

Figure 9. Regulation of STS-mediated caspase-independent cell death by SFK and Cdc42 signaling, Rab11a membrane trafficking, and Golgi membrane dynamics (A) Western blots of MCF7 and HeLa cell extracts showing phosphotyrosine patterns by using antibody PY20 after exposure of cells to STS + QVD-OPh for 4 h with or without pretreatment with PP2, representative of at least three experiments. Arrows designate proteins bands exhibiting SFK-dependent phosphorylation in STS-treated cell extracts. Grb2 protein levels: loading controls. (B and C) HeLa cells were transfected with the indicated siRNAs, or with golgin-160-GFP or golgin-84, or pretreated with SU6656 before exposure to DMSO+QVD-OPh or STS+QVD-OPh for 36 h. (B) Epifluorescence images of the nuclear morphology (Hoechst staining) showing that the caspase-independent death phenotype (chromatin condensation and nuclear shrinkage, arrows) is dramatically impaired by all conditions which inhibit ERC and Golgi fragmentation (arrowheads point to a typical interphase nucleus). Bar 10 μm. (C) Graph depicts the percentage of cells displaying apoptotic nuclei; means ± SD of three experiments (siCtl, siCdc42, and siRab11a; n > 1300 cells) or values from one experiment (siSFKs, siStx6, SU6656, and golgin-84, n > 150 cells; and golgin160, n > 30 cells).

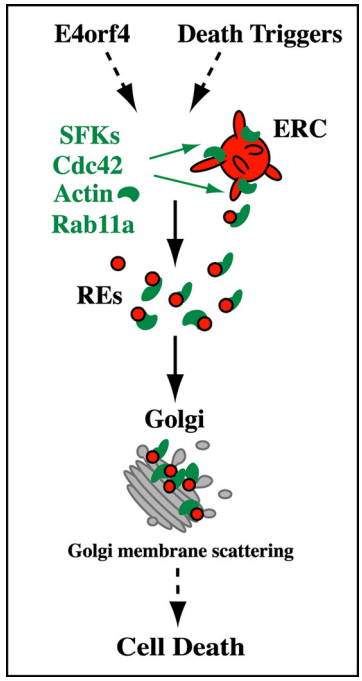

Figure 10. Working model: mobilization of REs in response to death triggers. We propose that the mobilization of REs via the coordinated actions of SFKs and Cdc42 at REs, which would control an actin-regulated Rab11a retrograde route at the endosome–Golgi interface, could be part of the upstream events that relay death signals to cellular organelles. REs could deliver signaling moieties controlling actin dynamics, which in turn would contribute to the remodeling of Golgi membranes (Golgi membrane scattering) whose dynamic changes regulate the progression of cell death. See *Discussion* for details.

could also contribute to the recruitment of REs to the Golgi based on evidence supporting a role for Cdc42-Par-aPKC complex in the localization of RE-associated proteins (Balklava *et al.*, 2007; Georgiou *et al.*, 2008; Harris and Tepass, 2008; Leibfried *et al.*, 2008). To our knowledge, however, the present study provides the first evidence for a role for Src, Yes and Cdc42 in the retrograde transport of endosomes to the Golgi complex (Johannes and Popoff, 2008).

Another important finding of this study concerns the redirection of RE trafficking in response to death signals and its role in Golgi dynamic changes. Changes in endosomal traffic during CD have been described mainly in response to death receptor signaling. In so-called type II cells requiring mitochondrial amplification of apical caspase signals, an initial wave of enhanced endocytosis is followed by a caspase-dependent dispersal of secretory membranes and in that context, apoptotic cell death was found to rely on endosomal traffic (Ouasti *et al.*, 2007; Degli Esposti, 2008; Matarrese *et al.*, 2008). Yet, evidence has been reported that receptor-independent death mechanisms induced by drugs such as STS neither stimulate endocytosis nor depend on the endosomal compartment (Matarrese *et al.*, 2008), the latter point being in apparent contradiction with our results. Those findings, however, were focused on changes in endocytosis and caspase-mediated cell death in human T cells (Matarrese *et al.*, 2008), whereas in our study, membrane trafficking from the ERC was found to regulate a more delayed caspase-independent death response in cancer cells. It is conceivable that the contribution of caspases and RE trafficking depends on the cellular context and that RE trafficking would substitute for caspases in the remodeling of the Golgi in cancer cells bearing dysfunctions in caspase pathways. Given that golgin-160, a caspase target involved in apoptotic Golgi disassembly (Mancini *et al.*, 2000), was found here to negatively regulate RE–Golgi interactions and

the ensuing scattering of Golgi membranes, it seems that RE trafficking and caspases could act on overlapping pathways for triggering death-promoting changes in Golgi dynamics. It is currently unclear how golgin-160 would intervene in RE-to-Golgi membrane transport and whether, like other golgins, it could regulate membrane tethering events that would limit vesicle fusion at the Golgi (Short *et al*., 2005), as suggested here by a reduction of RE–Golgi interactions. Yet, the recent discovery of a role for golgin-160 in Golgi positioning, directed secretion and cell polarity (Yadav *et al*., 2009), together with evidence supporting its death-promoting activity (Maag *et al*., 2005) emphasize the existence of novel cross-talks between the cell polarity machinery and death-promoting pathways. Furthermore, Cdc42 was also involved in Fas-enhanced membrane traffic leading to a polarization of REs around the Golgi (Degli Esposti *et al*., 2009). Together with our data, these suggest that Cdc42 plays a prevalent and unrecognized role in CD by virtue of its ability to control cell polarity and membrane traffic at numerous sites (Duncan and Peifer, 2008).

Elucidation of the mechanism whereby the increased RE-to-Golgi membrane transport and the ensuing changes in Golgi membrane dynamics can engage cell death is an important focus of future work. Protein transport by the retrograde route to the TGN is believed to provide a mechanism to establish pools of cargo for polarized secretion from specific regions of the cell (Johannes and Popoff, 2008). Therefore, the enhanced transport of REs to the Golgi complex could contribute to create connections between endocytic elements and exocytosis that could be instrumental for relaying death signals. RE-to-Golgi membrane transport was found here to stimulate Golgi membrane dynamics (fission), presumably as a result of a local delivery of remodeling factors that could promote actin assembly and ultimately Golgi membrane scattering (Carreno *et al*., 2004; Dubois *et al*., 2005). We are currently investigating the possibility that the ensuing release of Golgi-localized effectors could convey death signals, by analogy to the role of mitotic Golgi disassembly in cell division (Colanzi and Corda, 2007). Given that proteins and lipids with death-promoting activities are enriched at the Golgi membrane, it is conceivable that regulated changes in membrane dynamics allow their translocation to target compartments (Tembe and Henderson, 2007).

In conclusion, we propose that the mobilization of RE trafficking through a pathway involving SFKs, Cdc42, and Rab11a is part of the upstream core signaling networks that regulate CD by acting on the traffic of signaling moieties controlling the actin-dependent apoptotic remodeling of organelles.

ACKNOWLEDGMENTS

We are grateful to C. E. Machamer (Johns Hopkins University, Baltimore, MD); M. Way (London Research Institute, London, United Kingdom); N. Lamarche (McGill University, Montréal, QC, Canada); T. Balla and J. Lippincott-Schwartz (National Institutes of Health, Bethesda, MD); R. Y. Tsien (University of California, La Jolla, CA); H. M. McBride (University of Ottawa Heart Institute, Ottawa, ON, Canada); J. S. Brugge (Harvard Medical School, Boston, MA); M. Lowe (University of Manchester, Manchester, United Kingdom); L. Johannes (Institut Curie, Parie, France); and J. Landry, M. Caruso and N. Marceau (Laval University, Québec, QC, Canada) for providing critical molecular tools and reagents. We thank N. Marceau for critical discussion and C. St-Pierre and A. Loranger (Centre de Recherche en Cancérologie de l'Université Laval) for dedicated support and assistance in microscopic analyses. We are grateful to Ronald Hancock (Laval University) for editing this manuscript. This work was supported by the Canadian Institutes of Health Research operating grant MOP-49450 (to J.N.L.) and a maintenance Grant for the Cell imaging core facility. J.N.L. is a Senior Scholar of the Fonds de la Recherche en Santé du Québec (FRSQ) and M.-C.L. was supported by a studentship from the FRSQ.

REFERENCES

Balklava, Z., Pant, S., Fares, H., and Grant, B. D. (2007). Genome-wide analysis identifies a general requirement for polarity proteins in endocytic traffic. Nat. Cell Biol. *9*, 1066–1073.

Bolte, S., and Cordelieres, F. P. (2006). A guided tour into subcellular colocalization analysis in light microscopy. J. Microsc. *224*, 213–232.

Bruno, P., *et al*. (2009). Family at last: highlights of the first international meeting on proteins killing tumour cells. Cell Death Differ. *16*, 184–186.

Carreno, S., Engqvist-Goldstein, A. E., Zhang, C. X., McDonald, K. L., and Drubin, D. G. (2004). Actin dynamics coupled to clathrin-coated vesicle formation at the trans-Golgi network. J. Cell Biol. *165*, 781–788.

Casanova, J. E., Wang, X., Kumar, R., Bhartur, S. G., Navarre, J., Woodrum, J. E., Altschuler, Y., Ray, G. S., and Goldenring, J. R. (1999). Association of Rab25 and Rab11a with the apical recycling system of polarized Madin-Darby canine kidney cells. Mol. Biol. Cell *10*, 47–61.

Champagne, C., Landry, M. C., Gingras, M. C., and Lavoie, J. N. (2004). Activation of adenovirus type 2 early region 4 ORF4 cytoplasmic death function by direct binding to Src kinase domain. J. Biol. Chem. *279*, 25905–25915.

Chauvier, D., Ankri, S., Charriaut-Marlangue, C., Casimir, R., and Jacotot, E. (2007). Broad-spectrum caspase inhibitors: from myth to reality? Cell Death Differ. *14*, 387–391.

Chen, X. W., Inoue, M., Hsu, S. C., and Saltiel, A. R. (2006). RalA-exocyst-dependent recycling endosome trafficking is required for the completion of cytokinesis. J. Biol. Chem. *281*, 38609–38616.

Colanzi, A., and Corda, D. (2007). Mitosis controls the Golgi and the Golgi controls mitosis. Curr. Opin. Cell Biol. *19*, 386–393.

Costes, S. V., Daelemans, D., Cho, E. H., Dobbin, Z., Pavlakis, G., and Lockett, S. (2004). Automatic and quantitative measurement of protein-protein colocalization in live cells. Biophys. J. *86*, 3993–4003.

Degli Esposti, M. (2008). Organelle intermixing and membrane scrambling in cell death. Methods Enzymol. *442*, 421–438.

Degli Esposti, M., Tour, J., Ouasti, S., Ivanova, S., Matarrese, P., Malorni, W., and Khosravi-Far, R. (2009). Fas death receptor enhances endocytic membrane traffic converging into the Golgi region. Mol. Biol. Cell *20*, 600–615.

Derby, M. C., Lieu, Z. Z., Brown, D., Stow, J. L., Goud, B., and Gleeson, P. A. (2007). The trans-Golgi network golgin, GCC185, is required for endosome-to-Golgi transport and maintenance of Golgi structure. Traffic *8*, 758–773.

Diao, A., Rahman, D., Pappin, D. J., Lucocq, J., and Lowe, M. (2003). The coiled-coil membrane protein golgin-84 is a novel rab effector required for Golgi ribbon formation. J. Cell Biol. *160*, 201–212.

Doms, R. W., Russ, G., and Yewdell, J. W. (1989). Brefeldin A redistributes resident and itinerant Golgi proteins to the endoplasmic reticulum. J. Cell Biol. *109*, 61–72.

Dubois, T., Paleotti, O., Mironov, A. A., Fraisier, V., Stradal, T. E., De Matteis, M. A., Franco, M., and Chavrier, P. (2005). Golgi-localized GAP for Cdc42 functions downstream of ARF1 to control Arp2/3 complex and F-actin dynamics. Nat. Cell Biol. *7*, 353–364.

Duncan, M. C., and Peifer, M. (2008). Regulating polarity by directing traffic: Cdc42 prevents adherens junctions from crumblin' aPart. J. Cell Biol. *183*, 971–974.

Egea, G., Lazaro-Dieguez, F., and Vilella, M. (2006). Actin dynamics at the Golgi complex in mammalian cells. Curr. Opin. Cell Biol. *18*, 168–178.

Ferri, K. F., and Kroemer, G. (2001). Organelle-specific initiation of cell death pathways. Nat. Cell Biol. *3*, E255–E263.

Garofalo, T., Tinari, A., Matarrese, P., Giammarioli, A. M., Manganelli, V., Ciarlo, L., Misasi, R., Sorice, M., and Malorni, W. (2007). Do mitochondria act as "cargo boats" in the journey of GD3 to the nucleus during apoptosis? FEBS Lett. *581*, 3899–3903.

Georgiou, M., Marinari, E., Burden, J., and Baum, B. (2008). Cdc42, Par6, and aPKC regulate Arp2/3-mediated endocytosis to control local adherens junction stability. Curr. Biol. *18*, 1631–1638.

Gingras, M.-C., Champagne, C., Roy, M. A., and Lavoie, J. N. (2002). Cytoplasmic death signal triggered by Src-mediated phosphorylation of adenovirus E4orf4 protein. Mol. Cell. Biol. *22*, 41–56.

Graham, F. L., Smiley, J., Russell, W. C., and Nairn, R. (1977). Characteristics of a human cell line transformed by DNA from human adenovirus type 5. J. Gen. Virol. *36*, 59–74.

Grosshans, B. L., Ortiz, D., and Novick, P. (2006). Rabs and their effectors: achieving specificity in membrane traffic. Proc. Natl. Acad. Sci. USA *103*, 11821–11827.

Harris, K. P., and Tepass, U. (2008). Cdc42 and Par proteins stabilize dynamic adherens junctions in the Drosophila neuroectoderm through regulation of apical endocytosis. J. Cell Biol. *183*, 1129–1143.

Hicks, S. W., and Machamer, C. E. (2002). The NH2-terminal domain of Golgin-160 contains both Golgi and nuclear targeting information. J. Biol. Chem. *277*, 35833–35839.

Hicks, S. W., and Machamer, C. E. (2005). Golgi structure in stress sensing and apoptosis. Biochim. Biophys. Acta *1744*, 406–414.

Horgan, C. P., Oleksy, A., Zhdanov, A. V., Lall, P. Y., White, I. J., Khan, A. R., Futter, C. E., McCaffrey, J. G., and McCaffrey, M. W. (2007). Rab11-FIP3 is critical for the structural integrity of the endosomal recycling compartment. Traffic *8*, 414–430.

Huot, J., Lambert, H., Lavoie, J. N., Guimond, A., Houle, F., and Landry, J. (1995). Characterization of 45-kDa/54-kDa HSP27 kinase, a stress-sensitive kinase which may activate the phosphorylation-dependent protective function of mammalian 27-kDa heat-shock protein HSP27. Eur. J. Biochem. *227*, 416–427.

Johannes, L., and Popoff, V. (2008). Tracing the retrograde route in protein trafficking. Cell *135*, 1175–1187.

Jones, H. W., Jr., McKusick, V. A., Harper, P. S., and Wuu, K. D. (1971). George Otto Gey. (1899–1970). The HeLa cell and a reappraisal of its origin. Obstet. Gynecol. *38*, 945–949.

Jones, M. C., Caswell, P. T., and Norman, J. C. (2006). Endocytic recycling pathways: emerging regulators of cell migration. Curr. Opin. Cell Biol. *18*, 549–557.

Lanzetti, L. (2007). Actin in membrane trafficking. Curr. Opin. Cell Biol. *19*, 453–458.

Lavoie, J. N., Champagne, C., Gingras, M. C., and Robert, A. (2000). Adenovirus E4 open reading frame 4-induced apoptosis involves dysregulation of src family kinases. J. Cell Biol. *150*, 1037–1056.

Lavoie, J. N., Nguyen, M., Marcellus, R. C., Branton, P. E., and Shore, G. C. (1998). E4orf4, a novel adenovirus death factor that induces p53-independent apoptosis by a pathway that is not inhibited by zVAD-fmk. J. Cell Biol. *140*, 637–645.

Leibfried, A., Fricke, R., Morgan, M. J., Bogdan, S., and Bellaiche, Y. (2008). *Drosophila* Cip4 and WASp define a branch of the Cdc42-Par6-aPKC pathway regulating E-cadherin endocytosis. Curr. Biol. *18*, 1639–1648.

Li, S., Szymborski, A., Miron, M. J., Marcellus, R., Binda, O., Lavoie, J. N., and Branton, P. E. (2009). The adenovirus E4orf4 protein induces growth arrest and mitotic catastrophe in H1299 human lung carcinoma cells. Oncogene *28*, 390–400.

Lippincott-Schwartz, J., Donaldson, J. G., Schweizer, A., Berger, E. G., Hauri, H. P., Yuan, L. C., and Klausner, R. D. (1990). Microtubule-dependent retrograde transport of proteins into the ER in the presence of brefeldin A suggests an ER recycling pathway. Cell *60*, 821–836.

Livne, A., Shtrichman, R., and Kleinberger, T. (2001). Caspase activation by adenovirus e4orf4 protein is cell line specific and Is mediated by the death receptor pathway. J. Virol. *75*, 789–798.

Maag, R. S., Mancini, M., Rosen, A., and Machamer, C. E. (2005). Caspase-resistant Golgin-160 disrupts apoptosis induced by secretory pathway stress and ligation of death receptors. Mol. Biol. Cell *16*, 3019–3027.

Mallard, F., Antony, C., Tenza, D., Salamero, J., Goud, B., and Johannes, L. (1998). Direct pathway from early/recycling endosomes to the Golgi apparatus revealed through the study of shiga toxin B-fragment transport. J. Cell Biol. *143*, 973–990.

Mancini, M., Machamer, C. E., Roy, S., Nicholson, D. W., Thornberry, N. A., Casciola-Rosen, L. A., and Rosen, A. (2000). Caspase-2 is localized at the Golgi complex and cleaves golgin-160 during apoptosis. J. Cell Biol. *149*, 603–612.

Marcellus, R. C., Lavoie, J. N., Boivin, D., Shore, G. C., Ketner, G., and Branton, P. E. (1998). The early region 4 orf4 protein of human adenovirus type 5 induces p53-independent cell death by apoptosis. J. Virol. *72*, 7144–7153.

Matarrese, P., Manganelli, V., Garofalo, T., Tinari, A., Gambardella, L., Ndebele, K., Khosravi-Far, R., Sorice, M., Esposti, M. D., and Malorni, W. (2008). Endosomal compartment contributes to the propagation of CD95/Fas-mediated signals in type II cells. Biochem. J. *413*, 467–478.

Maxfield, F. R., and McGraw, T. E. (2004). Endocytic recycling. Nat. Rev. Mol. Cell Biol. *5*, 121–132.

Moreau, V., Frischknecht, F., Reckmann, I., Vincentelli, R., Rabut, G., Stewart, D., and Way, M. (2000). A complex of N-WASP and WIP integrates signalling cascades that lead to actin polymerization. Nat. Cell Biol. *2*, 441–448.

Ndozangue-Touriguine, O., Hamelin, J., and Breard, J. (2008). Cytoskeleton and apoptosis. Biochem. Pharmacol. *76*, 11–18.

Ouasti, S., Matarrese, P., Paddon, R., Khosravi-Far, R., Sorice, M., Tinari, A., Malorni, W., and Degli Esposti, M. (2007). Death receptor ligation triggers membrane scrambling between Golgi and mitochondria. Cell Death Differ. *14*, 453–461.

Parsons, M., *et al*. (2005). Spatially distinct binding of Cdc42 to PAK1 and N-WASP in breast carcinoma cells. Mol. Cell. Biol. *25*, 1680–1695.

Presley, J. F., Cole, N. B., Schroer, T. A., Hirschberg, K., Zaal, K. J., and Lippincott-Schwartz, J. (1997). ER-to-Golgi transport visualized in living cells. Nature *389*, 81–85.

Robert, A., Miron, M. J., Champagne, C., Gingras, M. C., Branton, P. E., and Lavoie, J. N. (2002). Distinct cell death pathways triggered by the adenovirus early region 4 ORF 4 protein. J. Cell Biol. *158*, 519–528.

Robert, A., Smadja-Lamere, N., Landry, M. C., Champagne, C., Petrie, R., Lamarche-Vane, N., Hosoya, H., and Lavoie, J. N. (2006). Adenovirus E4orf4 hijacks rho GTPase-dependent actin dynamics to kill cells: a role for endosome-associated actin assembly. Mol. Biol. Cell *17*, 3329–3344.

Sakurada, K., Uchida, K., Yamaguchi, K., Aisaka, K., Ito, S., Ohmori, T., Takeyama, Y., Ueda, T., Hori, Y., Ohyanagi, H., and et al. (1991). Molecular cloning and characterization of a ras p21-like GTP-binding protein (24KG) from rat liver. Biochem. Biophys. Res. Commun. *177*, 1224–1232.

Sandilands, E., Akbarzadeh, S., Vecchione, A., McEwan, D. G., Frame, M. C., and Heath, J. K. (2007a). Src kinase modulates the activation, transport and signalling dynamics of fibroblast growth factor receptors. EMBO Rep. *8*, 1162–1169.

Sandilands, E., Brunton, V. G., and Frame, M. C. (2007b). The membrane targeting and spatial activation of Src, Yes and Fyn is influenced by palmitoylation and distinct RhoB/RhoD endosome requirements. J. Cell Sci. *120*, 2555–2564.

Sandilands, E., Cans, C., Fincham, V. J., Brunton, V. G., Mellor, H., Prendergast, G. C., Norman, J. C., Superti-Furga, G., and Frame, M. C. (2004). RhoB and actin polymerization coordinate Src activation with endosome-mediated delivery to the membrane. Dev. Cell *7*, 855–869.

Sandilands, E., and Frame, M. C. (2008). Endosomal trafficking of Src tyrosine kinase. Trends Cell Biol. *18*, 322–329.

Saraste, J., and Goud, B. (2007). Functional symmetry of endomembranes. Mol. Biol. Cell *18*, 1430–1436.

Scaplehorn, N., Holmstrom, A., Moreau, V., Frischknecht, F., Reckmann, I., and Way, M. (2002). Grb2 and Nck act cooperatively to promote actin-based motility of vaccinia virus. Curr. Biol. *12*, 740–745.

Short, B., Haas, A., and Barr, F. A. (2005). Golgins and GTPases, giving identity and structure to the Golgi apparatus. Biochim. Biophys. Acta *1744*, 383–395.

Shtrichman, R., Sharf, R., Barr, H., Dobner, T., and Kleinberger, T. (1999). Induction of apoptosis by adenovirus E4orf4 protein is specific to transformed cells and requires an interaction with protein phosphatase 2A. Proc. Natl. Acad. Sci. USA *96*, 10080–10085.

Smadja-Lamere, N., Boulanger, M. C., Champagne, C., Branton, P. E., and Lavoie, J. N. (2008). JNK-mediated phosphorylation of paxillin in adhesion assembly and tension-induced cell death by the adenovirus death factor E4orf4. J. Biol. Chem. *283*, 34352–34364.

Soule, H. D., Vazguez, J., Long, A., Albert, S., and Brennan, M. (1973). A human cell line from a pleural effusion derived from a breast carcinoma. J. Natl. Cancer Inst. *51*, 1409–1416.

Tembe, V., and Henderson, B. R. (2007). Protein trafficking in response to DNA damage. Cell Signal *19*, 1113–1120.

Ullrich, O., Reinsch, S., Urbe, S., Zerial, M., and Parton, R. G. (1996). Rab11 regulates recycling through the pericentriolar recycling endosome. J. Cell Biol. *135*, 913–924.

van Ijzendoorn, S. C. (2006). Recycling endosomes. J. Cell Sci. *119*, 1679–1681.

Weigert, R., and Donaldson, J. G. (2005). Fluorescent microscopy-based assays to study the role of Rab22a in clathrin-independent endocytosis. Methods Enzymol. *403*, 243–253.

Wilcke, M., Johannes, L., Galli, T., Mayau, V., Goud, B., and Salamero, J. (2000). Rab11 regulates the compartmentalization of early endosomes required for efficient transport from early endosomes to the trans-Golgi network. J. Cell Biol. *151*, 1207–1220.

Wilson, G. M., Fielding, A. B., Simon, G. C., Yu, X., Andrews, P. D., Hames, R. S., Frey, A. M., Peden, A. A., Gould, G. W., and Prekeris, R. (2005). The FIP3-Rab11 protein complex regulates recycling endosome targeting to the cleavage furrow during late cytokinesis. Mol. Biol. Cell *16*, 849–860.

Yadav, S., Puri, S., and Linstedt, A. D. (2009). A primary role for Golgi positioning in directed secretion, cell polarity and wound healing. Mol. Biol. Cell 20, 1728–1736.